

Effect of microglial Pd1 on glial scar formation after spinal cord injury in mice

Received for publication, March 10, 2025, and in revised form, March 27, 2025. Published, Papers in Press, April 8, 2025.
<https://doi.org/10.1016/j.jbc.2025.108489>

Yunyun Cai¹, Zhihao Lin², Xin Shen¹, Ming Li¹, Lingyan Xing² , Tuo Yang³, and Gang Chen^{1,2,4,*} 

From the ¹Center for Basic Medical Research, Medical School of Nantong University, Co-innovation Center of Neuroregeneration, Nantong, Jiangsu Province, China; ²Key Laboratory of Neuroregeneration of Jiangsu and the Ministry of Education, Co-innovation Center of Neuroregeneration, NMPA Key Laboratory for Research and Evaluation of Tissue Engineering Technology Products, Nantong, Jiangsu Province, China; ³Department of Hand Surgery, China-Japan Union Hospital of Jilin University, Changchun, Jilin Province, China; ⁴Department of Anesthesiology, Affiliated Hospital of Nantong University, Nantong, Jiangsu Province, China

Reviewed by members of the JBC Editorial Board. Edited by Roger Colbran

The cross talk between microglia and astrocytes following spinal cord injury (SCI) greatly decides the prognosis. However, a comprehensive understanding of the molecular mechanisms by which microglia regulate astrocytic activity post-SCI is lacking. Programmed cell death protein 1 (Pdc1l, Pd1) plays a crucial role in modulating immune responses by exerting suppressive effects on microglia and peripheral immune cells within the central nervous system. Previous studies have shown the involvement of Pd1 in the pathogenesis of SCI; however, the role of microglial Pd1 in astrocytic activation and the following glial scar formation remains elusive. Here, we demonstrated that the pharmacological depletion of microglia using minocycline decreased the expression of tumor necrosis factor- α and interleukin-6 while concurrently increasing the expression of interleukin-10 following SCI, thereby facilitating motor function recovery in mice. We observed an increase in Pd1 expression in the injured spinal cord after SCI, with precise localization of Pd1 within microglia. Based on Pd1 knockout (KO) mice, we further revealed that Pd1 deficiency disrupted glial scar formation, leading to increased inflammation, impeded nerve regeneration, enlarged tissue damage, and compromised functional recovery following SCI. *In vitro* study showed that siRNA-mediated inhibition of Pd1 in microglia followed by lipopolysaccharide treatment significantly inhibited astrocyte migration and upregulated the secretion of tumor necrosis factor- α and CXCL9 from microglia, indicating that microglial Pd1 regulates glial scar formation through modulating the inflammatory microenvironment. Our study gains a new mechanistic insight into how microglial Pd1 decides the fate of SCI and promotes microglial Pd1 as a promising therapeutic target for SCI.

Spinal cord injury (SCI) is a profound trauma to the central nervous system (CNS) that often results in lifelong functional impairment (1). The pathophysiological process of SCI encompasses four stages: physical trauma, primary injury,

secondary injury, and glial scar formation (2). Traditionally, the prevailing perspective suggests that the glial scar exerts an inhibitory influence on nerve regeneration after SCI (3, 4). It is widely accepted that the mature glial scar serves as a physical barrier, impeding the regrowth and reconnection of nerve fibers to their original targets while also secreting extracellular matrix molecules that hinder axonal growth (5). However, in 2016, researchers reported that reducing the number of astrocytes to prevent glial scar formation did not effectively facilitate nerve fiber regeneration in the injured area (6). The deposition of chondroitin sulfate proteoglycans was unaffected by reactive astrocyte proliferation (6). Therefore, a comprehensive investigation into the mechanisms underlying glial scar formation following SCI will provide a crucial foundation for identifying novel therapeutic targets for this debilitating condition.

Microglia, which constitute approximately 10% of cells in the CNS (7), serve as immune cells (8) and actively contribute to maintaining CNS homeostasis through continuous interactions with neuronal and nonneuronal cell populations (9). The activation of microglia occurs rapidly after SCI, typically within 20 to 40 min following injury (10). After SCI, microglia gradually amplify inflammatory signals through the secretion of reactive oxygen species (ROS) (11) and proinflammatory cytokines such as tumor necrosis factor- α (TNF- α) (12), thereby aiding in the development of secondary injury. Additionally, microglia phagocytose debris through activation of the MyD88 pathway during the early stages of SCI. This process effectively mitigates inflammation and initiates the regeneration of oligodendrocytes (13). Microglia also secrete a plethora of nutrients, growth factors, and chemokines, which play a crucial role in modulating the internal milieu following SCI (14, 15). Furthermore, microglia also engage in intercellular communication to exert an indirect influence on the pathogenesis of SCI (16). The impact of microglia on astrocytes warrants the utmost attention, given the ubiquitous presence of astrocytes in the CNS and their pivotal role following SCI. Activated microglia can induce astrocytes to become

* For correspondence: Gang Chen, chengang6626@ntu.edu.cn.

Microglial Pd1 disrupts glial scar formation after SCI

neurotoxic by secreting interleukin-1 α (IL-1 α), TNF- α , and complement (C)1q (17) and promote reactive astrocyte-mediated tissue necrosis and induce cavitation through the Toll-like receptor (TLR)/MyD88 signaling pathway (18). Depletion of microglia using PLX5622 resulted in a reduction of glial fibrillary acidic protein (GFAP) mRNA levels at the lesion site and significantly suppressed astrocyte proliferation at the lesion edge (19, 20). After microglia depletion, the phosphorylation of STAT3 in astrocytes was impeded, resulting in dysregulated proliferation of the glial scar following SCI, the structural integrity became sparser, accompanied by a significant upregulation of inflammatory factors and exacerbated neuronal death (21). Microglia can suppress the P2Y₁ receptor of astrocytes *via* purinergic signaling, thereby attenuating astrocyte function in response to inflammatory mediators. This modulation promotes scar formation, restricts necrotic core expansion, facilitates blood–brain barrier repair, mitigates leukocyte infiltration (22) and significantly increases neuronal and oligodendrocyte survival to a considerable extent (23). The impact of microglia on astrocytes can be modulated in response to changes in the SCI environment, which is also associated with the rapid responsiveness of microglia to external signals.

Programmed cell death protein 1 (Pd1), also referred to as Cd274, is a transmembrane protein composed of 288 amino acids that plays a pivotal role as an immunosuppressive molecule within the immunoglobulin superfamily (24). Its expression is commonly observed in various immune cells, such as T cells, B cells, natural killer cells, dendritic cells, and macrophages, as well as other cell types, including microglia and neurons (25). Accumulating evidence suggests that Pd1 signaling plays a crucial role in not only immune system disorders but also central and peripheral nervous system disorders, including brain cancer (26), Alzheimer's disease (27), stroke (28), chronic pain (29), multiple sclerosis (30), and cognitive deficits (31). These findings underscore its potential as a promising therapeutic target for neurological disorders. Extensive investigations demonstrated an increase in the expression of Pd1 following SCI (32–35). Neuroinflammation following SCI involves the engagement of Pd1 signaling in T cells (36), as well as in macrophages and microglia (34). Current investigations into the regulatory mechanism of Pd1 signaling following SCI primarily focus on phenotypic alterations in macrophages and microglia. Specifically, Pd1 signaling has been demonstrated to suppress M1 polarization while promoting M2 polarization, thereby attenuating neuroinflammation in microglia and macrophages after SCI (33), SCI, suggesting the use of Pd1 targeting as a potential approach for treating SCI. However, the relationship between glial scar formation and Pd1, as well as the underlying mechanism of SCI in relation to Pd1 deficiency, remains poorly understood. In this study, our findings revealed the significant effect of microglial Pd1 on glial scar formation following SCI, elucidated the underlying mechanism and suggested that Pd1 could aid in the development of neural regeneration treatments for SCI patients.

Results

Microglia and astrocytes were located adjacent to each other after SCI

Increasing evidence suggests that microglia are pivotal cellular targets for injured spinal cord repair because of their involvement in glial scar formation, attenuation of parenchymal immune cell infiltration, and mitigation of neuronal and oligodendrocyte apoptosis during the first 2 weeks following SCI (23, 37, 38). The impact of microglia on astrocytes demands the utmost attention among the various factors under consideration. Microglia undergoes two phases of activation following SCI, with the initial phase occurring early in the injury and subsequent reactivation at 14 days post injury (dpi), coinciding with secondary neuronal damage (39). This reactivation may contribute to an augmented inflammatory response and scar formation, impeding neural tissue repair. Therefore, we selected the 14-day time point after SCI to investigate the relationship between microglia and astrocytes. Upon closer examination, we noted the physical proximity between microglia and astrocytes, along with spindle-shaped changes in the astrocytes surrounding microglia. The area surrounding microglia was occupied by astrocytes, and these cells worked together to enclose the lesion core (Fig. 1A). The proportion of appositions involving both astrocytes and microglia in the injured spinal cord increased from 0.65% to 63.2%, compared with the uninjured (normal) condition (Fig. 1, B and C). Therefore, our findings suggested that these two cell types interact during the process of SCI repair.

In the following study, to verify the specificity of Iba1 for microglia staining, we performed dual staining of Iba1 and Tmem119 in both uninjured spinal cords and at 14 dpi. The results demonstrated a high coexpression rate exceeding 95% (Fig. S1), confirming the specificity of Iba1 antibodies for labeling microglia in these contexts. Additionally, we observed that in healthy spinal cords, microglia predominantly reside in a resting state, characterized by small cell bodies, long processes, and numerous branches. Following SCI, nearly all microglia rapidly transitioned into an activated state, exhibiting significant morphological and functional alterations: enlarged cell bodies, shortened and thickened processes, and migration toward the injury site (Fig. S2).

The inhibition of microglial activation after SCI attenuated the SCI-induced inflammatory response and promoted functional recovery

Minocycline, a broad-spectrum tetracycline antibiotic, effectively suppresses microglial activation (40) and attenuates the expression of inflammatory factors in microglia (41). To explore the involvement of microglia in SCI, minocycline was administered at the time of SCI to suppress early microglial activation. Notably, minocycline treatment effectively attenuated microglial activation following SCI, as indicated by reductions in the Iba1 fluorescence intensity and extent of infiltration (Fig. 2, A and B). Furthermore, the behavioral outcomes demonstrated a significant increase in the recovery of SCI model mice treated with minocycline from day 7 to day

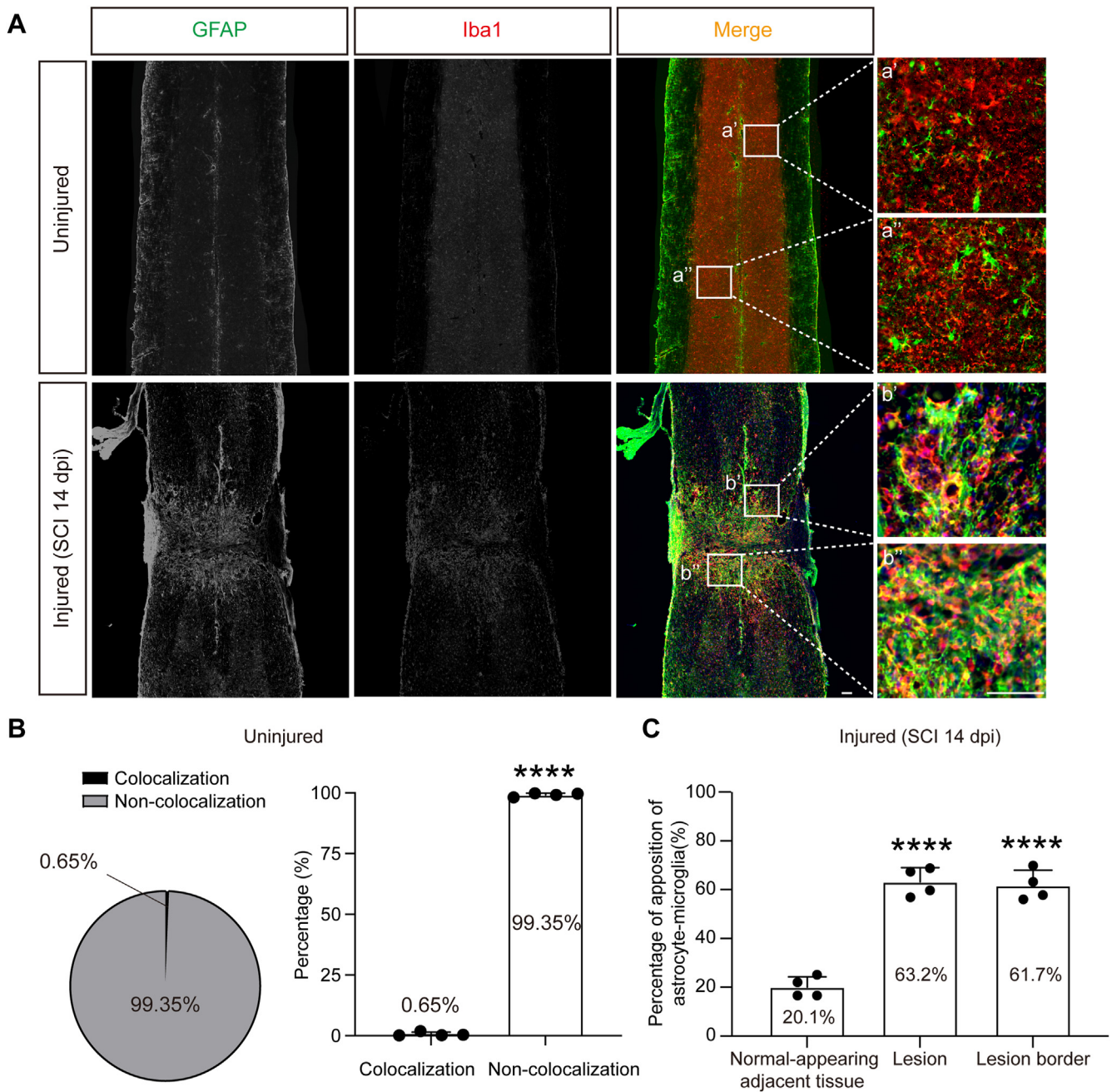


Figure 1. The relationship between microglia (Iba1+) and astrocytes (GFAP+) was investigated under normal conditions and 14 days post-SCI. A, representative immunofluorescence images showed that in the normal spinal cord, microglia and astrocytes were spatially distinct. In contrast, at the injury site, these cells accumulated at the edge of the lesion core, with most microglia and astrocytes in close proximity to each other. The scale bar represented 100 μ m. a'-a'', b'-b''. Enlarged images in the boxes of A and B. B, in the uninjured spinal cord, astrocytes, and microglia exhibited minimal colabeling. Left: pie chart. Right: columnar scatter plot. All data are presented as mean \pm SD. Statistical significance was determined using Student's *t* test and indicated by **** $p < 0.0001$ (unpaired *t* test (two-tailed), $t(6) = 173.7, p < 0.0001; n = 4$ mice per group). C, the apposition ratio of astrocytes and microglia increased to 63.2% at 14 days post-SCI at the lesion. At the lesion border, this ratio was 61.7% at 14 dpi, while in the normal-appearing adjacent tissue, it was 20.1% at 14 dpi. All data are presented as mean \pm SD. Statistical significance was indicated by **** $p < 0.0001$, as determined by one-way ANOVA (one-way ANOVA, $F(2, 9) = 79.56, p < 0.0001$; Normal-appearing adjacent tissue versus Lesion, $p < 0.0001$; Normal-appearing adjacent tissue versus Lesion border, $p < 0.0001; n = 4$ mice per group). dpi, days post injury; GFAP, glial fibrillary acidic protein; SCI, spinal cord injury.

14; however, no notable difference was observed on day 21, indicating that the therapeutic effect of minocycline on SCI may primarily manifest during the early stages, which is consistent with the prompt activation of microglia following SCI (Fig. 2C). As the efficacy of minocycline in promoting functional recovery following SCI has been substantiated, with

reported mechanisms encompassing antioxidant activity, attenuation of apoptosis, anti-inflammatory effects, and selective modulation of microglial activation, we assessed the concentrations of IL-1 β , IL-6, TNF- α (proinflammatory cytokines), and IL-10 (anti-inflammatory cytokines) in mice that received saline or minocycline injections. The levels of these

Microglial Pd1 disrupts glial scar formation after SCI

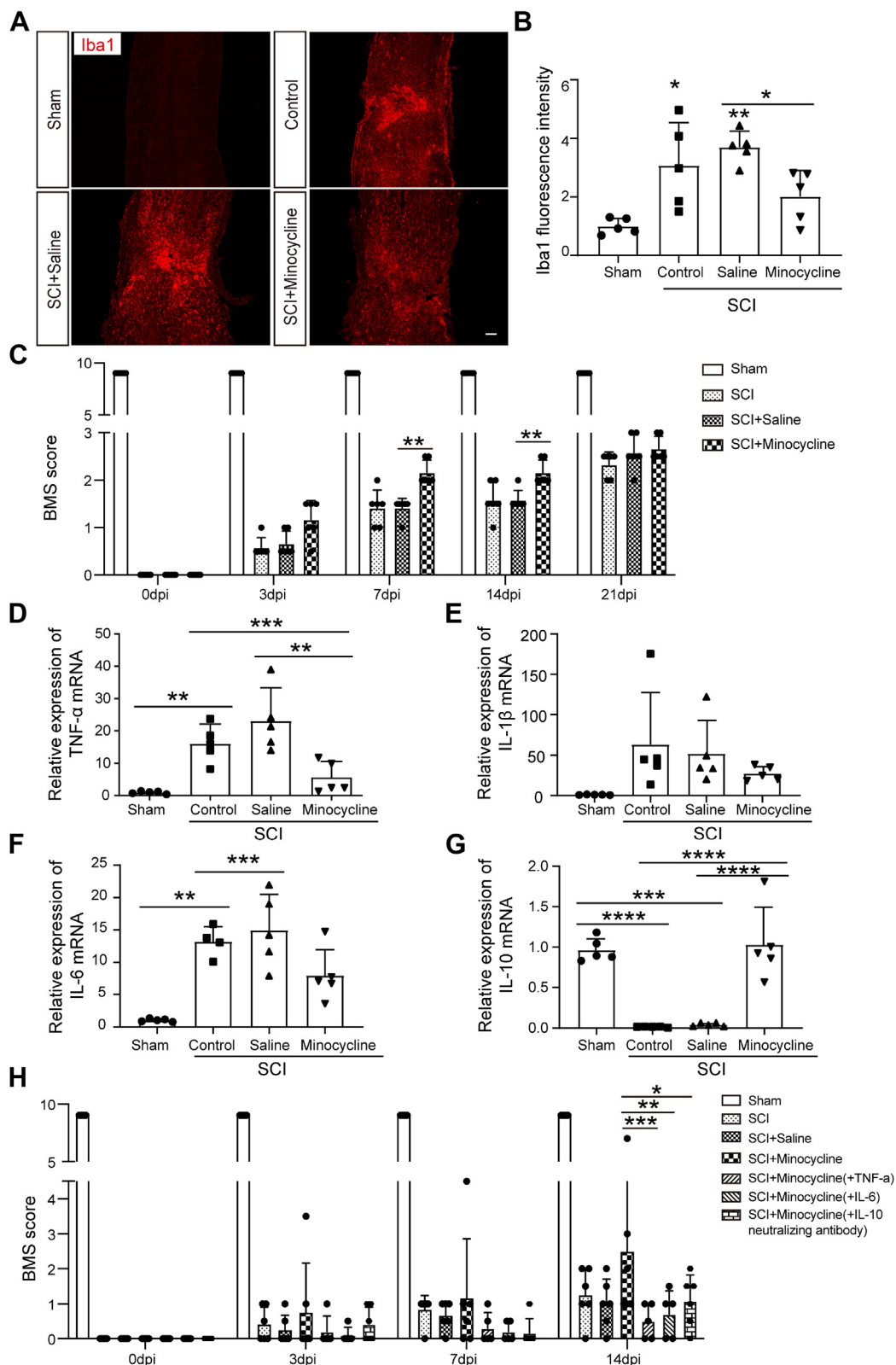


Figure 2. Microglia was involved in the functional recovery after SCI by regulating inflammatory response. *A*, immunofluorescence staining of Iba1 was conducted on the spinal cords of mice in sham group, control group, SCI + saline group and SCI + minocycline group. The sham group's mice underwent laminectomy without SCI and were sampled concurrently with the other groups. The scale bar represented 100 μ m. *B*, quantification of Iba1 immunostaining intensity in the spinal cords of mice in sham group, control group, SCI + saline group, and SCI + minocycline group. All data are presented as mean \pm SD. Statistical significance was indicated by * $p < 0.05$, ** $p < 0.01$, as determined by one-way ANOVA. *B*: one-way ANOVA, $F(3, 16) = 8.570$, $p = 0.0013$; sham versus control, $p = 0.0112$; sham versus SCI + saline, $p = 0.0012$; SCI + saline versus SCI + minocycline, $p = 0.0442$; $n = 5$ mice per group). *C*, locomotor recovery evaluated by the BMS score acquired at different time points after SCI in mice treated with nothing, saline, or minocycline. All data are presented as mean \pm SD. Statistical significance was indicated by ** $p < 0.01$, as determined by two-way ANOVA. *C*: two-way ANOVA, $F(12, 80) = 29.89$,

cytokines were assessed in the T9-10 spinal cord segment of mice at a 2-week post-SCI time point, which coincided with the peak behavioral response to minocycline treatment. Compared with the sham group, the injured group exhibited significantly elevated levels of TNF- α , IL-1 β , and IL-6 and reduced levels of IL-10. These findings suggested that inflammation plays a pivotal role in pathological progression following SCI. The quantitative real-time PCR (qPCR) results further validated that local administration of minocycline following SCI significantly ameliorated the inflammatory microenvironment, as evidenced by suppressed expression of proinflammatory cytokines (TNF- α and IL-6) while promoting the upregulation of an anti-inflammatory factor (IL-10). Although there was no significant difference in IL-1 β expression, it exhibited a slight upward trend (Fig. 2, D–G). The findings demonstrated that minocycline-induced depletion of microglia effectively ameliorated inflammation and facilitated the restoration of neurological function. In general, microglia are crucial for the pathological progression of SCI.

To further investigate whether the behavioral improvements in SCI induced by minocycline can be reversed by administering TNF- α or IL-6, or by antagonizing/knockdown of IL-10, we constructed an SCI model and administered TNF- α , IL-6, and IL-10 neutralizing antibody in conjunction with minocycline treatment. Results showed that at 14 dpi, administration of TNF- α , IL-6, and IL-10 neutralizing antibody significantly and partially reversed the behavioral improvements caused by minocycline (Fig. 2H). These findings suggested that minocycline's beneficial effects on SCI behavior may primarily involve inhibiting TNF- α , IL-6, and increasing IL-10, consistent with our qPCR results.

Pd1 was observed in both spinal neurons and microglia under normal conditions, while its upregulation specifically occurred in microglia following SCI in mice

Extensive research has revealed the prevalent presence of Pd1 in glial cells, neurons, and peripheral immune cells within the CNS (34, 42, 43). To further investigate Pd1 expression in the spinal cord, we used a double immunofluorescence staining technique to colocalize Pd1 with four major cell markers: NeuN for neurons, GFAP for astrocytes, Iba1 for microglia, and adenomatous polyposis coli clone 1 (APC) for oligodendrocytes. Pd1 was predominantly expressed in both spinal neurons and microglia in naïve mice, as evidenced by the presence of the respective markers NeuN and Iba1, while showing negligible colocalization with GFAP or APC (Fig. 3A).

To better ascertain the predominant expression of Pd1 in neurons and microglia, we conducted further data analysis on their colocalization patterns. The results revealed that 78.6% of Pd1 was expressed by neurons, while a lower percentage (14.3%) was expressed in microglia; conversely, only a minor fraction of Pd1 was expressed in astrocytes (5.9%) and oligodendrocytes (1.2%) (Fig. 3B). These findings indicated that under normal circumstances, Pd1 was specifically found in neurons and microglia.

To further investigate the alteration in Pd1 expression in microglia following SCI, we collected spinal cords surrounding the lesion sites at 14 dpi and conducted immunohistochemical staining to assess Pd1 expression in microglia. The expression of Pd1 in microglia was significantly upregulated after SCI compared to the sham group, as evidenced by the colabeling of two antibodies, Pd1 and Iba1 (Fig. 4, A and B). Furthermore, statistical analysis revealed that the expression of Pd1 in microglia reached 82.3% following SCI (Fig. 4C).

To confirm the microglial origin of Pd1 following SCI, we initially conducted quantitative fluorescence analysis on the costaining of Pd1 and Iba1, revealing a positive correlation between the fluorescence expression levels of Pd1 and Iba1 post-SCI (Fig. 4D). Subsequently, we employed minocycline, an inhibitor of microglial activation. As depicted in Figure 4E, treatment with minocycline resulted in reduced C-X3-C Motif Chemokine Receptor 1 (CX3CR1) expression. Collectively, these findings strongly supported the idea that Pd1 predominantly originates from microglia after SCI.

Pd1 expression was upregulated following SCI, and its deficiency was linked to impaired locomotor recovery

Compelling evidence suggested that the involvement of Pd1 was crucial in CNS disorders (32, 44), including SCI (33). To elucidate the expression pattern of Pd1 in SCI, we quantified the protein and mRNA expression of Pd1 using immunofluorescence staining and qPCR at multiple time points, including sham, 7-, 14-, 21-, and 28-days post-SCI. The fluorescence intensity of Pd1 was observed to undergo a 3- to 4-fold enhancement following SCI (Fig. 5, A and B). Our findings also revealed a significant increase in Pd1 mRNA expression, with an increase greater than 6-fold observed at 7 dpi, followed by a greater than 11-fold increase at 14 days and a remarkable 16-fold increase at the 28-day time point after SCI (Fig. 5C).

Subsequently, an SCI model was used to assess locomotor recovery in both Pd1 KO mice and WT mice. The distribution

$p < 0.0001$; 7 days, SCI + saline versus SCI + minocycline, $p = 0.0017$; 14 days, SCI + saline versus SCI + minocycline, $p = 0.0099$; $n = 6$ mice per group). D–G, minocycline treatment reduced SCI-induced IL-6 and TNF- α mRNA expression and increased IL-10 mRNA expression in the injured spinal cord. All data are presented as mean \pm SD. Statistical significance was indicated by ** $p < 0.01$, *** $p < 0.001$, **** $p < 0.0001$, as determined by one-way ANOVA. D: one-way ANOVA, $F(3, 16) = 13.27$, $p = 0.0001$; sham versus control, $p = 0.0078$; sham versus SCI + saline, $p = 0.0002$; SCI + saline versus SCI + minocycline, $p = 0.0022$; $n = 5$ mice per group. E: one-way ANOVA, $F(3, 16) = 2.660$, $p = 0.0834$; $n = 5$ mice per group. F: one-way ANOVA, $F(3, 15) = 13.48$, $p = 0.0002$; sham versus control, $p = 0.0013$; sham versus SCI + saline, $p = 0.0002$; sham versus SCI + minocycline, $p = 0.0014$; control versus SCI + minocycline, $p = 0.0001$; $n = 4$ –5 mice per group. G: one-way ANOVA, $F(3, 16) = 26.44$, $p < 0.0001$; sham versus control, $p < 0.0001$; sham versus SCI + saline, $p = 0.0001$; control versus SCI + minocycline, $p < 0.0001$; SCI + saline versus SCI + minocycline, $p < 0.0001$; $n = 5$ mice per group). H, locomotor recovery evaluated by the BMS score acquired at different time points after SCI in mice treated with nothing, saline, minocycline, minocycline (+TNF- α), minocycline (+IL-6), and minocycline (+IL-10 neutralizing antibody). All data are presented as mean \pm SD. Statistical significance was indicated by * $p < 0.05$, ** $p < 0.01$, *** $p < 0.001$, as determined by two-way ANOVA. H: two-way ANOVA, $F(18, 134) = 1.336$, $p = 0.1754$; 14 days, SCI + minocycline versus SCI + minocycline (+TNF- α), $p = 0.0002$; SCI + minocycline versus SCI + minocycline (+IL-6), $p = 0.0014$; SCI + minocycline versus SCI + minocycline (+IL-10 neutralizing antibody), $p = 0.0160$; $n = 5$ to 6 mice per group). BMS, Basso Mouse Scale; IL-6, interleukin-6; SCI, spinal cord injury; TNF- α , tumor necrosis factor- α .

Microglial Pd1 disrupts glial scar formation after SCI

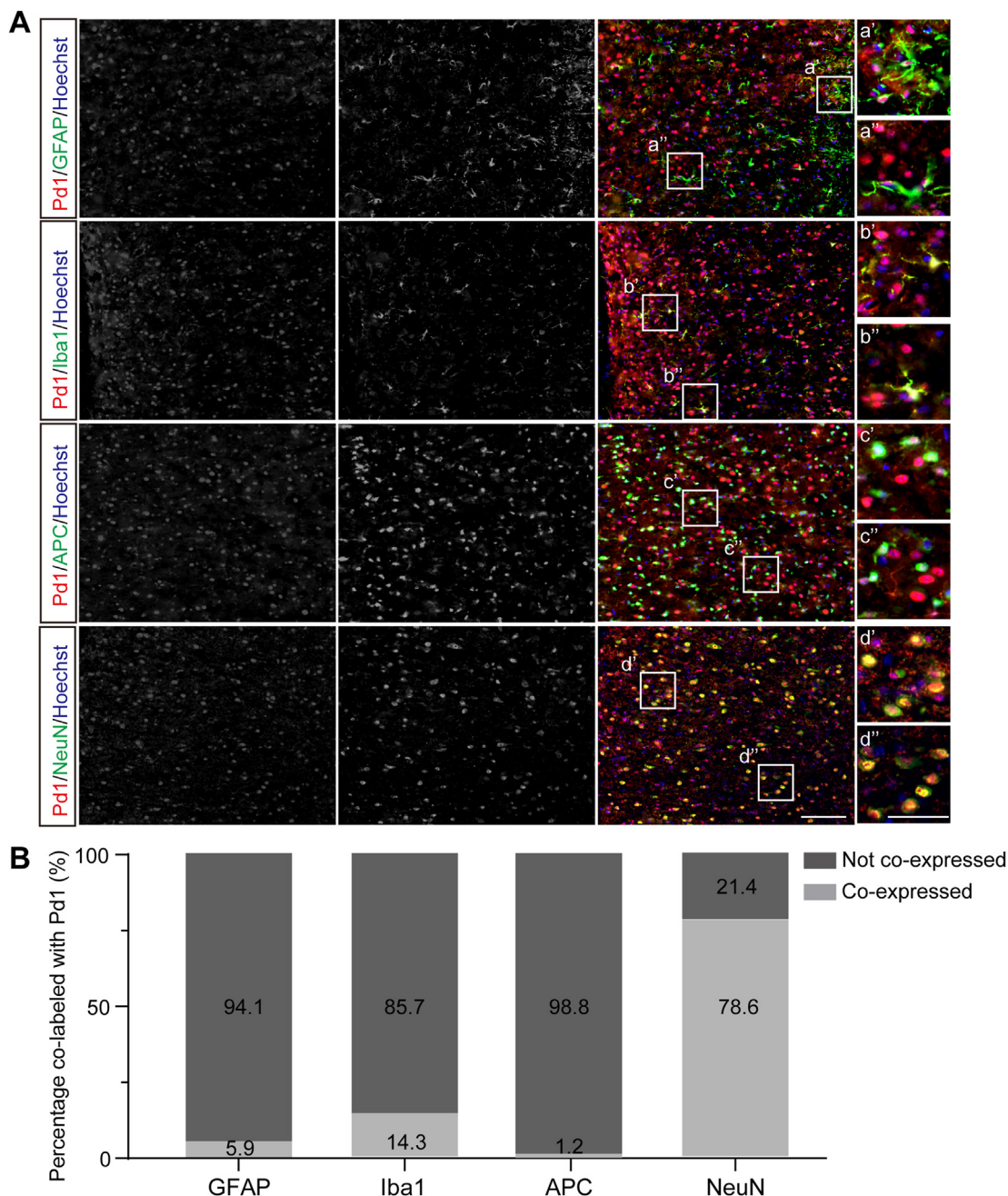


Figure 3. The distribution of Pd1 in the spinal cords of naive mice was examined. *A*, the colocalization of Pd1 (red) with different cell markers was investigated by double staining with GFAP (green), Iba1 (green), APC (green), and NeuN (green). Nuclear staining (Hoechst) was displayed in blue. The scale bar represented 100 μ m. The enlarged images in the boxes of a-d were shown as a'-d' and a''-d''. The scale bar represented 50 μ m. *B*, percentages of Pd1 colocalization with different cell types in the spinal cords of naive mice were determined: 78.6% of Pd1 expression was observed in neurons, 14.3% in microglia, 5.9% in astrocytes, while hardly any expression was detected in oligodendrocytes. APC, adenomatous polyposis coli clone 1; GFAP, glial fibrillary acidic protein; Pd1, programmed cell death protein 1.

of Pd1 in the spinal cord was examined in both WT mice and Pd1 KO mice, revealing a negligible presence of Pd1 in the latter group, confirming the successful generation of transgenic mice (Fig. 5, D and E). The success and reliability of the transgenic mice were further demonstrated by the results obtained from agarose gel electrophoresis (Fig. 5F). We further assessed motor function recovery in both WT mice and Pd1 KO mice following SCI using the Basso Mouse Scale (BMS). Although the Pd1 KO mice exhibited slightly lower BMSs at

1-week post injury, this difference did not reach statistical significance compared to that of the WT mice. However, the absence of Pd1 resulted in impaired locomotor recovery between two and four weeks after SCI compared with that in WT mice, indicating a delayed process of locomotor recovery following SCI (Fig. 5G).

Taken together, these findings indicated that Pd1 exerted a beneficial effect on the restoration of motor function following SCI in mice.

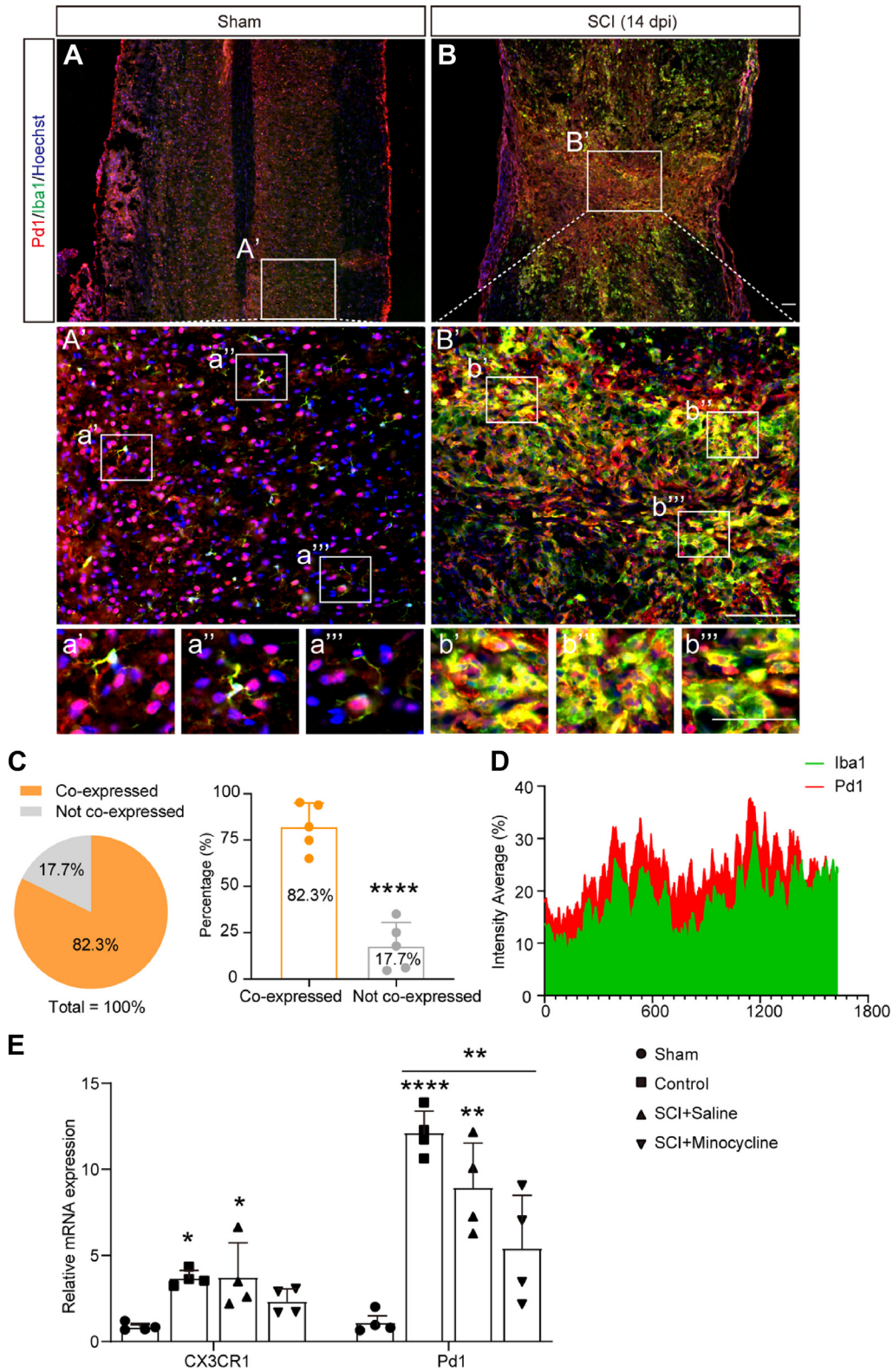


Figure 4. A significant upregulation of Pd1 expression in microglia was observed after SCI. A and B, the coexpression of Pd1 and Iba1 was observed in intact spinal cords as well as at 14 dpi in mice, demonstrating a significant upregulation of Pd1 specifically within Iba1+ cells following SCI. In the sham group, mice underwent laminectomy without SCI, and samples were collected on day 14. A'–B', enlarged images in the boxes of A and B. The white dotted line established a visual connection between the small image enclosed within the box and its corresponding enlarged version. The scale bar represented 100 μ m. a'–b', a''–b'', a'''–b'''. Enlarged images in the boxes of A and B. The scale bar represented 50 μ m. C, the coexpression of Pd1 in microglia was observed at a rate of 82.3% in the injured spinal cord following SCI. Left: pie chart. Right: columnar scatter plot. All data are presented as mean \pm SD. Statistical significance was determined using Student's *t* test and indicated by *****p* < 0.0001 (unpaired *t* test (two-tailed), *t* (8) = 7.951, *p* < 0.0001; *n* = 5 mice per group). D, quantitative analysis of Pd1 and Iba1 fluorescence intensity, along with their coexpression correlation with FUOM expression, was

Microglial Pd1 disrupts glial scar formation after SCI

Pd1 deficiency induced microglial activation and disrupted glial scar formation

The activation of microglia has a crucial function in initiating inflammatory immune responses, while the Pd1 signaling pathway potentially regulates microglia-associated signaling pathways across diverse pathological conditions (44). As mentioned earlier, microglia displayed noticeable enlargement of cells and withdrawal of extensions following SCI. Moreover, our study demonstrated the expression of Pd1 in microglia, particularly under pathological conditions. Therefore, at the conclusion of the 28-day behavioral testing period, when Pd1 mRNA expression levels reached their zenith after SCI, we further investigated the potential impact of Pd1 depletion on microglial activation following SCI in mice. Immunohistochemistry was once again used to assess potential alterations in the distribution of Iba1+ microglia within the injured spinal cords of WT mice and Pd1 KO mice in the SCI model. In the Pd1 KO SCI mouse model, there was a significant increase in the number of Iba1+ microglia, which exhibited an increase in size and increased fluorescence intensity (Fig. 6, A–C).

As previously stated, the formation of glial scars after SCI significantly impacts patient outcomes (45); however, the role of Pd1 in glial scar formation remains unclear. The fluorescence intensity and dimensions of the glial scar were assessed through immunohistochemical staining for GFAP. Pd1 KO mice had a smaller glial scar, characterized by a well-defined border with robust immunofluorescence reactivity of GFAP surrounding the core lesion at 4 weeks post-SCI. Additionally, Pd1 KO mice exhibited a notable decrease in the population of GFAP+ cells within the glial scar area (Fig. 6, D–F). Pd1 KO mice exhibited a significant decrease in both tissue lesion size and cell count, which was further confirmed through H&E staining analysis (Fig. 6, G–I).

Pd1 deficiency impeded neuronal survival after SCI

The recovery of neurological function following SCI relies on the integrity and plasticity of neural circuitry, which can be compromised by axonal damage and subsequent neuronal demise (46). The loss of mature neurons constitutes a prominent etiological factor underlying functional impairments after SCI (47). Immunofluorescence analysis, utilizing β -III tubulin as a specific marker for neurons, was used to assess the neuronal population near the injury site. The findings demonstrated a notable decrease in the number of neurons at the site of injury in Pd1 KO mice compared to WT mice on day 28 following SCI (Fig. 6, J–L). These findings suggested that disruption of Pd1 hampered nerve regeneration following SCI.

The downregulation of Pd1 in microglia inhibited glial scar formation by increasing the expression of inflammatory factors and chemokines

To gain further insight into the underlying mechanism by which microglial Pd1 disrupts glial scar formation, we conducted *in vitro* culture experiments employing microglia. Initially, we used different concentrations (20 nM and 50 nM) of Pd1 siRNA to effectively suppress the expression of Pd1 mRNA in cultured microglia. The efficacy of Pd1 siRNA-mediated knockdown was subsequently validated, as shown in Figure 7A. Pd1 mRNA expression was significantly reduced by 53.9% following treatment with Pd1 siRNA (20 nM) and by 67.5% following treatment with Pd1 siRNA (50 nM) compared to that in the control group treated with negative control (NC) siRNA. Based on the observed efficiency, while both concentrations of Pd1 siRNA resulted in essentially the same knockdown of Pd1 mRNA, the degree of knockdown stability was more pronounced with 50 nM siRNA. Therefore, we selected this concentration for subsequent experiments.

The present study demonstrated that SCI elicited a persistent inflammatory response. To simulate microglial activation in response to an inflammatory stimulus, cultured microglia were treated with lipopolysaccharide (LPS). LPS, an endotoxin located on the outer membrane of Gram-negative bacteria, can activate TLR4 to initiate microglial activation (48). Upon binding to TLR4 on microglia, LPS triggers downstream signaling pathways including nuclear factor- κ B (NF- κ B) and p38 MAPK signaling pathways (48, 49), resulting in the release of various inflammatory mediators such as TNF- α , IL-6, and nitric oxide (50). This induced inflammatory response serves as a model for simulating inflammatory processes within the nervous system. Microglia treated with LPS (0 μ g/ml or 5 μ g/ml) were cultured at 37 °C for 24 h. The expression levels of granulocyte colony-stimulating factor (G-CSF), intercellular cell adhesion molecule-1 (ICAM-1, CD54), and the inflammatory factors IL-6 and TNF- α significantly increased upon exposure to LPS. Additionally, there was a notable upregulation in the expression of four chemokines (CXCL10, CCL12, CXCL9, and CCL5). These findings indicated successful activation of microglia.

To elucidate the molecular mechanism underlying the inhibitory effect of Pd1 knockdown on microglial astrocyte migration and glial scar formation, a mouse cytokine array consisting of 40 distinct cytokines/chemokines was utilized to analyze microglia treated with NC siRNA + LPS or Pd1 siRNA + LPS. The comparison of various treatments on protein samples revealed a significant increase in the levels of one inflammatory factor (TNF- α) and one chemokine (CXCL9) following treatment with Pd1 siRNA + LPS compared to those in the group treated with NC siRNA + LPS, as indicated by the

performed to elucidate the relationship between these markers. *E*, the administration of minocycline effectively suppressed microglial activation and concomitantly attenuated the expression of Pd1. All data are presented as mean \pm SD. Statistical significance was indicated by * p < 0.05, ** p < 0.01, **** p < 0.0001 as determined by one-way ANOVA. *E* (CX3CR1): one-way ANOVA, F (3, 12) = 6.084, p = 0.0093; sham versus control, p = 0.0210; sham versus SCI + saline, p = 0.0186; n = 4 mice per group) mRNA expression, accompanied by a corresponding decrease in Pd1 *E* (Pd1): one-way ANOVA, F (3, 12) = 18.40, p < 0.0001; sham versus control, p < 0.0001; sham versus SCI + saline, p = 0.0018; control versus SCI + minocycline, p = 0.0063; n = 4 mice per group). In this experiment, we respectively compared the expression of CX3CR1 and Pd1 expression across four distinct experimental groups, and we put them all together just to make it more intuitive. dpi, days post injury; Pd1, programmed cell death protein 1; SCI, spinal cord injury.

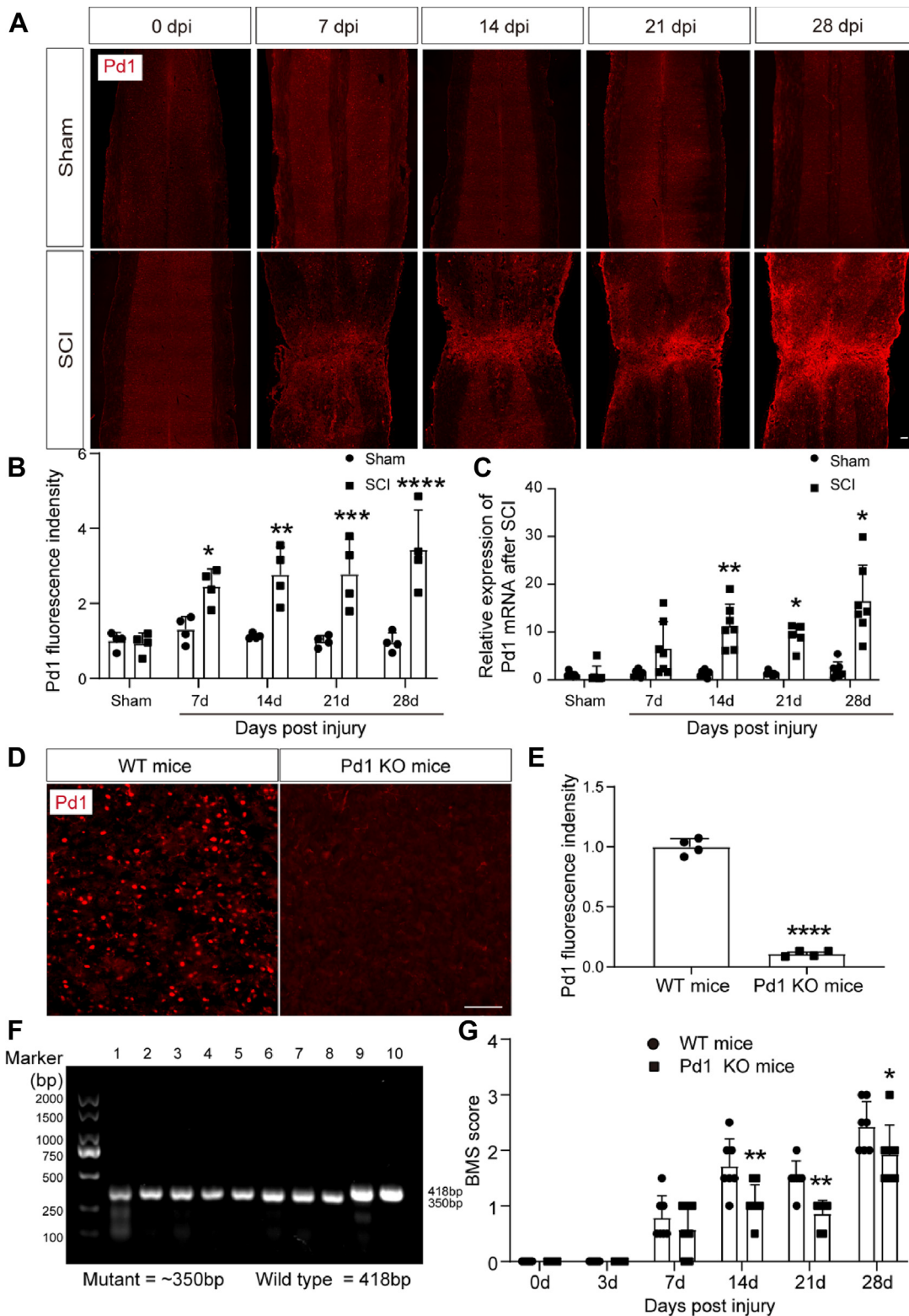


Figure 5. The expression of Pd1 in the injured spinal cord following SCI and the impact of Pd1 deficiency on motor recovery in mice with SCI. *A*, representative images illustrating Pd1 immunostaining (red) in the spinal cord of sham mice (day 0, day 7, day 14, day 21, and day 28) and mice with SCI (day 0, day 7, day 14, day 21, and day 28) were presented, accompanied by a scale bar indicating a length of 100 μ m. In the sham group, mice underwent laminectomy without SCI. *B*, the statistical analysis revealed significant differences in the intensity of Pd1 between sham mice (day 0, day 7, day 14, day 21, and day 28) and SCI mice (day 0, day 7, day 14, day 21, and day 28). In the sham group, mice underwent laminectomy without SCI. All data are presented as mean \pm SD. Statistical significance was determined by two-way ANOVA and indicated by * p < 0.05, ** p < 0.01, *** p < 0.001, **** p < 0.0001. (*B*: two-way ANOVA, $F(4, 30) = 5.771$, $p = 0.0014$; sham (7 days) versus 7 dpi, $p = 0.0326$; sham (14 days) versus 14 dpi, $p = 0.0012$; sham (21 days) versus 21 dpi, $p = 0.0004$; sham (28 days) versus 28 dpi, $p < 0.0001$; $n = 4$ mice per group). *C*, Pd1 mRNA levels were quantified using qPCR in T9-10 spinal cords from mice at various time points following SCI. The analysis revealed a significant upregulation of Pd1 mRNA expression from 7 to 28 days after SCI compared to the sham group. All data are presented as mean \pm SD. Statistical significance was determined by one-way ANOVA and indicated by * p < 0.05, ** p < 0.01. *C*: two-

Microglial Pd1 disrupts glial scar formation after SCI

cytokine levels (Fig. 7, B and C). In summary, these findings suggested that microglial Pd1 plays a role in glial scar formation by regulating the expression of inflammatory factors and chemokines.

The downregulation of Pd1 in microglia inhibited astrocyte migration

To deepen our understanding of how microglial Pd1 influences glial scar formation, we conducted an *in vitro* coculture experiment using microglia and astrocytes. Two groups of astrocytes were treated with conditioned medium from microglia transfected with either NC siRNA + LPS (5 µg/ml) or Pd1 siRNA (50 nM) + LPS (5 µg/ml). Scratch assay analysis was performed at 6-, 12-, 24-, 36-, and 48-h post treatment. Both groups exhibited migration toward the center; however, a significant difference was observed specifically at the 48-h time point (Fig. 8). Specifically, comparing the group treated with NC siRNA + LPS to the group treated with Pd1 siRNA + LPS revealed that reduced Pd1 expression in microglia significantly weakened astrocyte migration, suggesting that microglial Pd1 plays a crucial role in modulating glial scar formation.

Discussion

Despite extensive research on the impact of Pd1 on microglial polarization during injured spinal cord repair (33, 34, 36), the precise role and mechanism of Pd1 in microglia-mediated glial scar formation remain unclear. This research clarified the importance of microglial Pd1 in facilitating glial scar formation, modulating cytokine expression, and promoting motor function recovery following SCI. The current study suggested that communication between Pd1 in microglia and the glial scar might be an important process in SCI-induced worse motor dysfunction.

SCI models are essential not only for assessing the efficacy of therapeutic interventions but also for gaining a deeper understanding of the underlying molecular pathways involved. Significant advancements have been made in SCI modeling since Allen first developed the initial hit contusion model in 1911 (51). Variations among these models include the choice of animal species, site-specific injury locations, and other factors. Although cervical SCI is more prevalent clinically, the selection of the T9-10 level in this study was based on the survival rate and widespread utilization associated with thoracic SCI. According to the diverse mechanisms of injury, the SCI model can be categorized into contusion, compression, stretch, dislocation, transection, and chemical injury. Previous studies have demonstrated that the compression model of SCI

is more suitable for investigating postinjury scarring (52); hence, we selected this model.

Microglia, as resident immune cells of the CNS, play pivotal roles in CNS development, homeostasis maintenance, and the response to injury and infection (53–55). For decades, the involvement of microglia in the pathophysiology of SCI has remained elusive, focusing mainly on the fact that they mediate inflammatory responses post-SCI (56). Similarly, our findings indicated that the depletion of microglia after SCI through minocycline treatment increased the levels anti-inflammatory factors while simultaneously decreasing the levels of pro-inflammatory factors following SCI. Furthermore, our findings revealed improved motor function in mice with SCI following microglial depletion. Minocycline, a clinically available antibiotic and anti-inflammatory agent, has been extensively demonstrated to effectively target various secondary injury mechanisms in SCI. These mechanisms encompass inflammation, oxidative stress mediated by free radicals, glutamate excitotoxicity, calcium influx, mitochondrial dysfunction, ischemia-reperfusion injury, hemorrhage-induced damage, and edema formation (57). Minocycline has exhibited the capacity to (1) inhibit microglial activation and proliferation (58); (2) protect neurons against oxidative stress and scavenging of free radicals (59), prevent glutamate-induced neuronal apoptosis (60), shield neurons from toxicity induced by bleeding events (61); (3) inhibit oligodendrocyte apoptosis while enhancing functional recovery following SCI (62). These findings further substantiate minocycline's targeted impact on microglial inhibition. To ensure experimental reliability and provide additional evidence supporting minocycline's specific targeting toward microglia within the CNS, it will be interesting for future research to include additional inhibitors of microglia or utilize minocycline for treating and observing alterations in other types of glial cells and neurons *in vitro*. The secretion of inflammatory cytokines, such as ROS and TNF- α , by microglia following SCI initiates the sequential amplification of inflammatory signals that contribute to secondary SCI damage; however, minocycline treatment can ameliorate this phenomenon by attenuating the activation of microglia following SCI. Timely elimination of microglia post-SCI has the potential to partially ameliorate the impairments caused by SCI. Pharmacological depletion of spinal microglia using a CSF1R inhibitor (PLX5622) has been shown to effectively mitigate chronic inflammation and neurodegeneration, thereby facilitating the restoration of neurological function (23). However, microglia exhibit sensitivity and multipotency in response to SCI. Localized administration of colony-stimulating factor to increase microglial proliferation

way ANOVA, $F(4, 46) = 9.275, p < 0.0001$; sham (14 days) versus 14 dpi, $p = 0.0052$; sham (21 days) versus 21 dpi, $p = 0.0104$; sham (28 days) versus 28 dpi, $p = 0.0100$; $n = 6$ to 7 mice per group). D, representative immunofluorescence images demonstrated the distribution of Pd1 in the spinal cord of both WT mice and Pd1 KO mice. The scale bar represented 100 µm. E, quantification of Pd1 immunostaining intensity in the spinal cords of both WT mice and Pd1 KO mice. All data are presented as mean \pm SD. Statistical significance was indicated by **** $p < 0.0001$, as determined by Student's *t* test. F, unpaired *t* test (two-tailed), $t(6) = 24.57, p < 0.0001$; $n = 4$ mice per group). G, identification of Pd1 KO mice through gel electrophoresis analysis. H, locomotor recovery was assessed using the BMS score at different time points after SCI in WT and Pd1 KO mice. All data are presented as mean \pm SD. Statistical significance was determined by two-way ANOVA and indicated by * $p < 0.05$, ** $p < 0.01$. I: two-way ANOVA; 14 days, $p = 0.0036$; 21 days, $p = 0.0036$; 28 days, $p = 0.0400$; $n = 7$ mice per group). BMS, Basso Mouse Scale; dpi, days post injury; Pd1, programmed cell death protein 1; qPCR, quantitative real-time PCR; SCI, spinal cord injury.

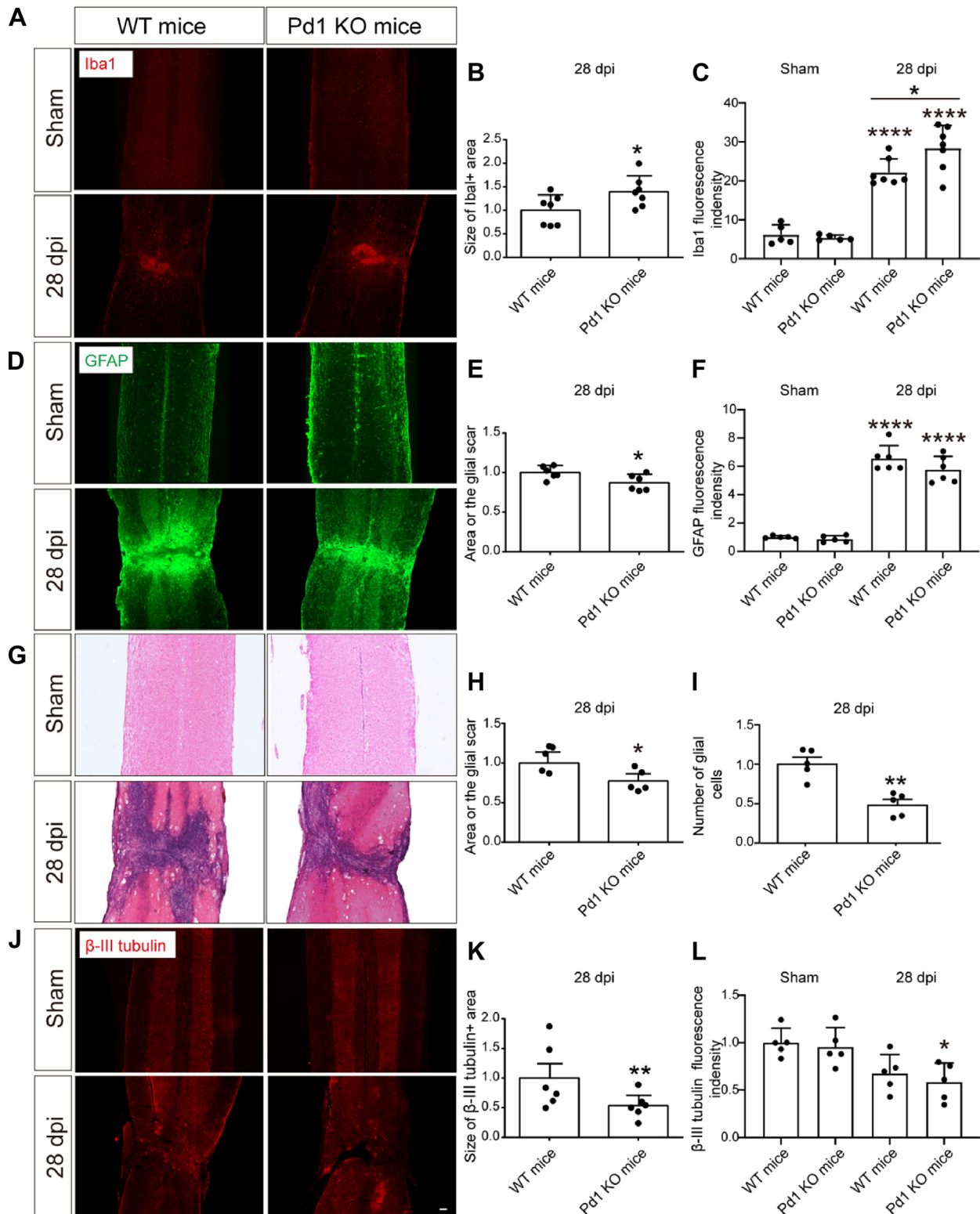


Figure 6. Pd1 deficiency promoted inflammation diffusion, hindered glial scar formation, augmented the size of the injury site and cell death, and impaired nerve regeneration following SCI. Immunofluorescence staining was conducted to evaluate the expression levels of Iba1 (A), GFAP (D), and β -III tubulin (J) in both sham-operated and SCI-injured WT and Pd1 KO mice at 28 days post injury. The immunostaining area and intensity of Iba1 (B and C), GFAP (E and F), and β -III tubulin (K and L) were quantified in the spinal cord of WT mice and Pd1 KO mice. All data are presented as mean \pm SD. Statistical significance was determined using Student's *t* test and indicated by * $p < 0.05$, ** $p < 0.01$, **** $p < 0.0001$. B: unpaired *t* test (two-tailed), $t(12) = 2.262$, $p = 0.0431$; $n = 7$ mice per group; C: one-way ANOVA, $F(3, 20) = 51.43$, $p < 0.0001$; WT mice (28 dpi), $p < 0.0001$, Pd1 KO mice (28 dpi), $p < 0.0001$, WT mice (28 dpi) versus Pd1 KO mice (28 dpi), $p = 0.0339$; $n = 5/7$ mice per group; E: unpaired *t* test (two-tailed), $t(10) = 2.423$, $p = 0.0359$; $n = 6$ mice per group; F: one-way ANOVA, $F(3, 18) = 102.2$, $p < 0.0001$; WT mice (28 dpi), $p < 0.0001$, Pd1 KO mice (28 dpi), $p < 0.0001$, Pd1 KO mice (28 dpi) versus WT mice (28 dpi), $p = 0.0339$; $n = 6$ mice per group; G-I: the hematoxylin-eosin staining revealed a significant decrease in glial scar formation, and the number of cells in Pd1 KO mice compared to WT mice. H: unpaired *t* test (two-tailed), $t(10) = 3.520$, $p = 0.0055$; $n = 6$ mice per group; I: unpaired *t* test (two-tailed), $t(10) = 3.520$, $p = 0.0055$; $n = 6$ mice per group; K: unpaired *t* test (two-tailed), $t(10) = 3.520$, $p = 0.0055$; $n = 6$ mice per group; L: one-way ANOVA, $F(3, 16) = 5.840$, $p = 0.0069$; Pd1 KO mice (28 dpi), $p = 0.0319$; $n = 5$ mice per group.

Microglial Pd1 disrupts glial scar formation after SCI

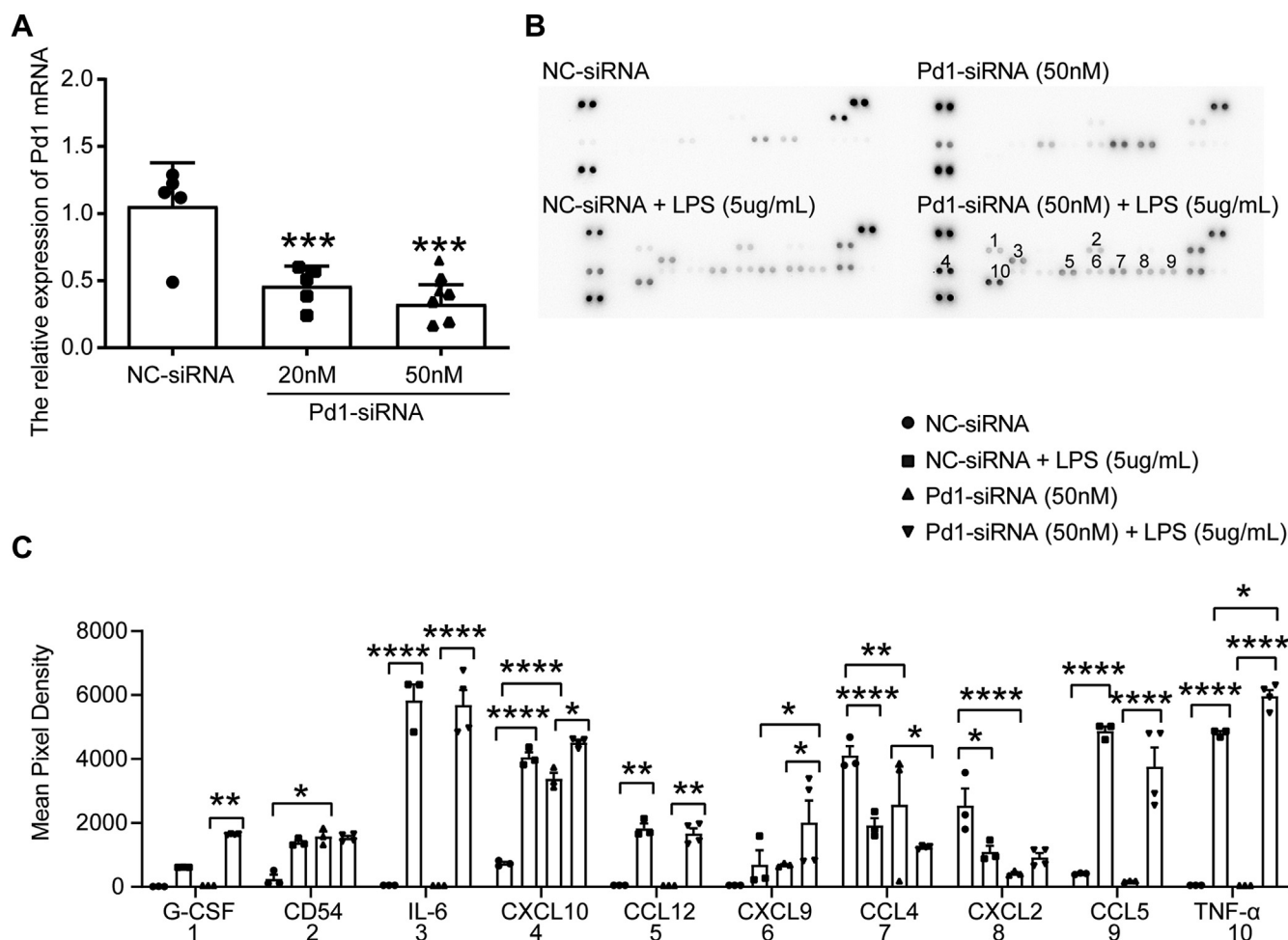


Figure 7. Cytokine array analysis revealed Pd1-dependent cytokines and chemokines in LPS-treated microglia. *A*, qPCR showing the decreased Pd1 mRNA in the microglia after Pd1 siRNA (20 nM and 50 nM) treatment for 48 h. All data are presented as mean \pm SD. Statistical significance was indicated by $**p < 0.01$, $***p < 0.001$, as determined by one-way ANOVA. *A*: ANOVA, $F(2, 12) = 15.32$, $p = 0.0005$; NC siRNA versus Pd1 siRNA 20 nM, $p = 0.0022$; NC siRNA versus Pd1 siRNA 50 nM, $p = 0.0004$; $n = 5$ wells per group). *B*, array membranes of protein expression among NC siRNA, NC siRNA + LPS (5 μ g/ml), Pd1 siRNA (50 nM), and Pd1 siRNA (50 nM) + LPS (5 μ g/ml) groups in culture medium for microglia. *C*, the expression of one colony-stimulating factor (G-CSF), one intercellular cell adhesion molecule (CD54), two inflammatory factors (IL-6 and TNF- α), and four chemokines (CXCL10, CCL12, CXCL9, and CCL5) significantly increased following LPS treatment, while the expression of one chemokine (CCL4) decreased. A significant increase in the expression of one inflammatory factor (TNF- α) and one chemokine (CXCL9) after treatment with Pd1 siRNA + LPS. All data are presented as mean \pm SD. Statistical significance was indicated by $*p < 0.05$, $**p < 0.01$, $***p < 0.001$, $****p < 0.0001$, as determined by two-way ANOVA. (Figure 6C: two-way ANOVA; G-CSF, NC siRNA versus Pd1 siRNA + LPS, $p = 0.0016$, Pd1 siRNA versus Pd1 siRNA + LPS, $p = 0.0021$; CD54, NC siRNA versus Pd1 siRNA, $p = 0.0245$, NC siRNA versus Pd1 siRNA + LPS, $p = 0.0185$; IL-6, NC siRNA versus NC siRNA + LPS, $p < 0.0001$, NC siRNA versus Pd1 siRNA + LPS, $p < 0.0001$, NC siRNA + LPS versus Pd1 siRNA, $p < 0.0001$; Pd1 siRNA versus Pd1 siRNA + LPS, $p < 0.0001$; CXCL10, NC siRNA versus NC siRNA + LPS, $p < 0.0001$, NC siRNA versus Pd1 siRNA, $p < 0.0001$, NC siRNA versus Pd1 siRNA + LPS, $p = 0.0017$, NC siRNA + LPS versus Pd1 siRNA, $p = 0.0012$; Pd1 siRNA versus Pd1 siRNA + LPS, $p = 0.0017$; CXCL9, NC siRNA versus Pd1 siRNA + LPS, $p < 0.0001$, NC siRNA + LPS versus Pd1 siRNA + LPS, $p = 0.0156$, Pd1 siRNA versus Pd1 siRNA + LPS, $p = 0.0145$; CCL4, NC siRNA versus NC siRNA + LPS, $p < 0.0001$, NC siRNA versus Pd1 siRNA, $p = 0.0062$, NC siRNA versus Pd1 siRNA + LPS, $p < 0.0001$, Pd1 siRNA versus Pd1 siRNA + LPS, $p = 0.0143$; CXCL2, NC siRNA versus NC siRNA + LPS, $p = 0.0121$, NC siRNA versus Pd1 siRNA, $p < 0.0001$, NC siRNA versus Pd1 siRNA + LPS, $p = 0.0017$; CCL5, NC siRNA versus NC siRNA + LPS, $p < 0.0001$, NC siRNA versus Pd1 siRNA + LPS, $p < 0.0001$, NC siRNA + LPS versus Pd1 siRNA, $p < 0.0001$, Pd1 siRNA versus Pd1 siRNA + LPS, $p < 0.0001$; TNF- α , NC siRNA versus NC siRNA + LPS, $p < 0.0001$, NC siRNA versus Pd1 siRNA + LPS, $p < 0.0001$, NC siRNA + LPS versus Pd1 siRNA, $p < 0.0001$, NC siRNA + LPS versus Pd1 siRNA + LPS, $p = 0.0442$, Pd1 siRNA versus Pd1 siRNA + LPS, $p < 0.0001$; $n = 3-4$ separate experiments per group). G-CSF, granulocyte colony-stimulating factor; IL-6, interleukin-6; LPS, lipopolysaccharide; NC, negative control; Pd1, programmed cell death protein 1; qPCR, quantitative real-time PCR; siRNA, small interfering RNA; TNF- α , tumor necrosis factor-alpha.

promotes tissue preservation and facilitates motor recovery (23, 38). A recent study revealed that temporary activation of microglia and subsequent release of fibronectin and multiple

peptidase inhibitors in neonatal mice with SCI promote the restoration of spinal cord connectivity while resolving inflammation (63). These findings further substantiated the

mice at 28 days post SCI. All data are presented as mean \pm SD. Statistical significance was determined using Student's *t* test and indicated by $*p < 0.05$, $**p < 0.01$. The scale bar represented 100 μ m. *H*: unpaired *t* test (two-tailed), $t(8) = 2.732$, $p = 0.0258$; $n = 5$ mice per group; Figure 6I: unpaired *t* test (two-tailed), $t(8) = 4.953$, $p = 0.0011$; $n = 5$ mice per group). In the sham group of this experiment, WT mice (left) and Pd1 KO mice (right) underwent only the removal of the lamina without sustaining SCI. Samples were collected on day 28. dpi, days post injury; GFAP, glial fibrillary acidic protein; Pd1, programmed cell death protein 1; SCI, spinal cord injury.

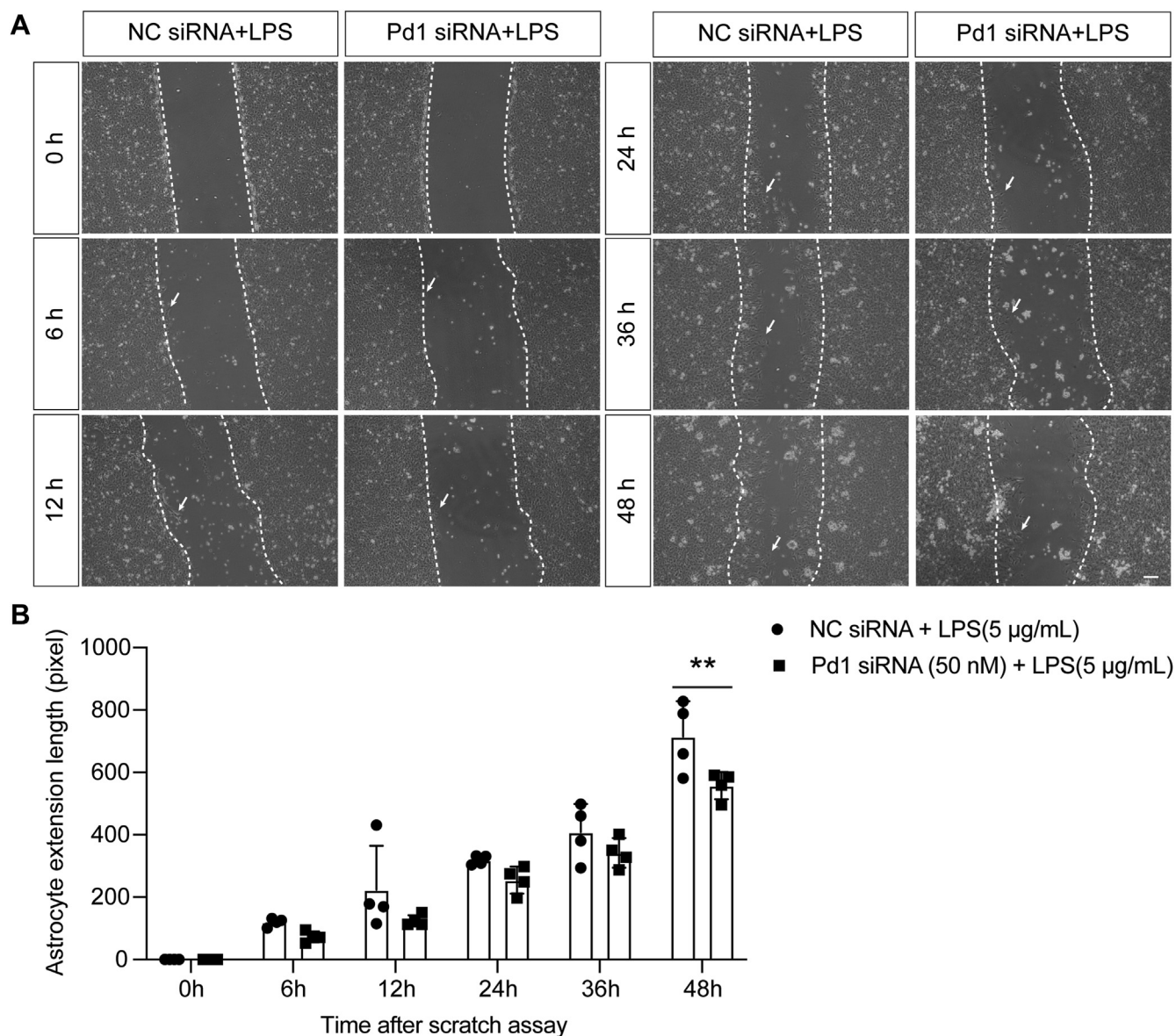


Figure 8. The downregulation of Pd1 in microglia inhibited astrocyte migration *in vitro*. *A*, continuous monitoring of astrocytes following scratch injury. Images were acquired at 0-, 6-, 12-, 24-, 36-, and 48-h post scratch. The white arrows denoted the specific regions within the visual field where astrocytes exhibited the highest degree of migration. The scale bar represented 100 µm. *B*, quantification of the migration distance of astrocytes in the scratch migration assay. All data are presented as mean ± SD. Statistical significance was indicated by ** $p < 0.01$, as determined by two-way ANOVA. ($F(5, 36) = 1.378, p = 0.2557$; NC siRNA + LPS versus Pd1 siRNA + LPS, 48 h, $p = 0.0076$; $n = 4$ wells per group). LPS, lipopolysaccharide; siRNA, small interfering RNA; NC, negative control; Pd1, programmed cell death protein 1.

advantageous role of microglia in recovery from SCI. Therefore, it is imperative to gain a comprehensive understanding of the alterations that occur in microglia following SCI and to elucidate the underlying molecular mechanisms involved.

SCI induces the formation of glial scars at the injury site, characterized by astrocyte hypertrophy, proliferation, and migration and the upregulation of GFAP, vimentin, and nestin expression (64). The glial scar is recognized as a pivotal factor contributing to profound and irreversible neurological impairment. It forms physical barriers that impede axonal extension and hinder nerve repair (65); in addition, reactive astrocytes exert detrimental effects through specific stimulatory signaling cascades, such as increased production of

inflammatory cytokines (66), ROS (67), and extracellular excitatory glutamate (68). Accumulating evidence suggests that rather than preventing recovery after CNS injury, the glial scar contributes to recovery by effectively isolating healthy tissue from diseased tissue. For example, the double KO of GFAP and vimentin in mice resulted in a reduction in glial scar formation but an increase in hemorrhage and tissue damage (69). Conditional ablation of reactive astrocytes or selective depletion of astrocytes through knockdown of the STAT3 pathway also resulted in increased edema, inflammation, oligodendrocyte death, demyelination, and exacerbation of functional impairment (70). Furthermore, reactive astrocytes in the glial scar secrete various bioactive substances, including

Microglial Pd1 disrupts glial scar formation after SCI

laminin, which plays a crucial role in creating a favorable microenvironment for axon regeneration (6). These processes indicate that reactive astrocytes play a key role in the formation of glial scars and are indispensable for facilitating functional recovery following CNS injury. In our experiments, we observed that Pd1 KO mice exhibited reduced glial scar formation and impaired motor function recovery following SCI.

Extensive microglial proliferation and accumulation between fibrous and astrocytic scars were observed 4 to 14 days post-SCI (23). Our results demonstrated that microglia and astrocytes exhibited close spatial proximity, with astrocytes predominantly located at the periphery of the microglia, collectively enclosing the lesion core on the 14th day post-SCI. This observation suggested a potential interplay between these two cell types during glial scar formation. Microglia has been demonstrated to regulate the formation of astrocytic glial scars by controlling astrocyte proliferation, adhesion, and gliosis (20). Depletion of microglia disrupts the density and continuous boundaries of fibrotic and astrocytic scars, resulting in extensive inflammation within the lesion core (23). Furthermore, microglia contribute to the absence of fibrosis and astrocyte scarring, thereby coordinating scar-free healing following neonatal SCI (63). Given the critical role of astrocytes and microglia in coordinating the resolution of neuroinflammation to maintain CNS homeostasis, it is imperative to explore the influence of microglia on astrocytes following injury. This intriguing observation also introduces a new pathway for forthcoming research pursuits. Our results demonstrated that, in addition to the injury site, astrocytes and microglia in adjacent normal areas were also affected during SCI. This phenomenon may be attributed to multiple factors. Firstly, postinjury inflammatory mediators such as cytokines and chemokines disseminate to surrounding tissues, thereby activating adjacent astrocytes and microglia and initiating an inflammatory response. Secondly, the injury induces excessive glutamate release, which spreads to neighboring regions, leading to excitotoxicity and subsequent activation of surrounding glial cells. Thirdly, free radicals generated after injury propagate to surrounding tissues, causing oxidative stress and further activating adjacent glial cells. Fourthly, glial cells interact with extracellular signaling molecules *via* gap junctions, transmitting signals from the damaged area to neighboring cells and triggering a chain reaction. Lastly, damage disrupts the blood–spinal cord barrier, permitting the infiltration of inflammatory cells and molecules from the bloodstream into surrounding tissues, thereby activating glial cells. Additionally, secondary injury mechanisms, such as ischemia and edema, extend to adjacent areas, affecting normal cells.

The function of Pd1 in the immune system has been extensively investigated (71), and recent studies have provided compelling evidence for its involvement in various CNS functions, including stroke (72), SCI (35, 36), cognitive function (73, 74), and pain perception (29, 75). Our study extended these findings by demonstrating the upregulation of Pd1 expression in the spinal cord at the site of injury following SCI and revealed that motor function recovery was compromised in Pd1 KO mice. These results suggest the potential

involvement of Pd1 in the pathogenesis and progression of SCI. Pd1 is widely expressed in T cells, macrophages, microglia, neurons, and melanoma cells (34, 42, 76, 77). Furthermore, our findings provided additional support for the notion that Pd1 expression was predominantly observed in microglia following SCI. Previous findings have demonstrated that Pd1 expression was predominantly observed in macrophages/microglia following SCI, and the absence of Pd1 significantly impacted the early fate determination of macrophages/microglia, promoting their differentiation toward the M1 phenotype (34). Additionally, it has been demonstrated that the exacerbation of SCI is caused by Pd1 deficiency, which influences the reprogramming of NG2-glia and activation of the NgR/RhoA/ROCK signaling pathway (35). Pd1 was instrumental in the subacute stage of SCI by enhancing Foxp3 expression and anti-inflammatory activity in infiltrating Tregs, thereby counteracting the impact of proinflammatory macrophages and microglia (36). Notably, the existing studies on the role of Pd1 in SCI predominantly focused on inflammation and neuronal changes, while there is a dearth of literature exploring the impact of Pd1 in microglia on glial scar formation post injury. Our study pioneered the notion that down-regulated expression of Pd1 in microglia following SCI disrupts glial scar formation. Although our results have demonstrated the normal expression of Pd1 in microglia, as well as the specific upregulation of Pd1 in microglia following SCI, these findings provided sufficient evidence to confirm that microglia was the primary site of Pd1 expression after SCI. However, due to time and financial constraints, our selection of experimental mice was suboptimal. Therefore, future studies should focus on generating transgenic mice with targeted KO of Pd1 specifically in microglia to enhance the robustness and completeness of our experimental design.

Pd1 may regulate the activation, cytokine secretion, and differentiation of microglia following SCI through negative feedback signaling (34). To investigate the impact of Pd1 expression in microglia on glial scar formation following SCI, we subsequently examined alterations in inflammatory cytokine release by Pd1-depleted microglia. Currently, numerous studies have been conducted on *in vitro* cell models of SCI, employing three primary methods: (1) inducing mouse microglia with LPS to establish an *in vitro* model of SCI (78–81); (2) utilizing H₂O₂ treatment on neurons-dorsal spinal cord (RN-dsc) to construct an *in vitro* model of SCI (82); (3) employing modified myelinating cultures as an *in vitro* model of SCI (83). Given the robust *in vivo* evidence supporting the role of microglial Pd1 in regulating glial scar formation through modulation of inflammatory response, we employed an *in vitro* approach using LPS stimulation to mimic neuroinflammation pharmacologically, which was more aligned with the objectives of our research. Moreover, LPS-stimulated microglia have been extensively utilized to investigate pathogenesis, including SCI (84–86). According to the cytokine array results of the supernatants from microglia treated with NC siRNA + LPS or Pd1 siRNA + LPS, in addition to TNF- α , increased expression of other cytokines and chemokines (CXCL9) was observed, indicating that these inflammatory

factors could participate in SCI. TNF- α exerts a dual effect on astrocytes following SCI, potentially promoting migration and scarring or inhibiting migration depending on specific conditions. Evidence has shown that treating the scratched astrocyte monolayer with TNF- α significantly inhibits the limited cell proliferation observed at the wound site (87). Studies also have demonstrated that inhibiting TNF- α reduces the inflammatory response in the injured area following SCI, thereby promoting motor function recovery, enhancing axonal and myelin preservation, and decreasing glial scar formation post injury (46). Currently, the precise mechanisms by which CXCL9 influences glial scar formation following SCI and its direct impact on astrocyte migration remain unclear. Future studies could focus on elucidating the role of CXCL9 in these processes.

A comprehensive understanding of the formation, configuration, and functionality of the glial scar represents a promising strategy for successful recovery after SCI. Moreover, microglia are regarded as potential contenders for cellular therapy. This investigation revealed a novel therapeutic approach for SCI by means of microglial Pd1-mediated glial scar formation, thereby providing fresh insights into the regulatory mechanisms governing glial scarring.

Experimental procedures

Animals

Male Pd1 knockout (KO) (Pdcd-1 $^{-/-}$) mice were obtained from the Shanghai Model Organisms Center (https://www.modelorg.com/portal/article/index/id/3577/post_type/3.html), while male C57BL/6 mice were acquired from the Laboratory Animal Center of Nantong University. The experimental mice were approximately 8 weeks old. The mice were housed in a dedicated facility with controlled lighting, humidity, and temperature conditions. Unrestricted access to both food and water was provided to all the mice. All animal experiments were approved by the Society for Animal Ethics of Nantong University (permission no. S20220303-005).

Agarose gel electrophoresis

We isolated genomic DNA from mouse ears using the Mouse Genotyping Kit (Ubigen, YK-MG-100). The extracted DNA was subjected to PCR amplification in accordance with specific reaction conditions and reaction system guidelines provided by the company's transgenic mice purchase report. Detailed primer information can be found in Table 1. A 1.2% agarose (Sigma-Aldrich, A9539) gel was prepared, and the DNA products were directly loaded at a volume of 5 to 10 μ l per well along with markers and corresponding positive and negative controls. Based on the identification

report, the PCR bands were compared, leading to the derivation of conclusions.

SCI model

Mice were placed on a warming device and anaesthetized with isoflurane (RWD Life Science, R510-22-10) using a small animal anesthesia system. The surgical procedure was performed under an operating microscope, and the T9-10 spinal cord was compressed for 5 s using No. 5 Dumont forceps (FST) with a polished tip measuring 0.5 mm in width and no spacer. The criteria for successful model establishment were as follows: immediately following the clamping injury operation, mice exhibited edema and hemorrhage; the spinal cord crush resulted in the appearance of a hyperemic mark; their behavioral motor score dropped to 0 points upon awakening from anesthesia; hind limb motor function was lost, resulting in urinary retention; hind limbs dragged on the ground and tails could not be raised. After surgery, 1 ml of saline was intraperitoneally injected into each mouse to replenish body fluids, and manual bladder massage was performed twice daily until spontaneous excretion was restored. In each experimental design, mice in the sham group were matched for age, sex, and strain with those in the other experimental groups. Notably, the sham surgery group underwent only laminectomy without SCI and was sampled concurrently with the other groups.

Analysis of microglia morphology

The analysis of microglial morphology was conducted using ImageJ software. Specific plugins in the software were utilized to transform the high-magnification images into binary format. Following the processes of outlining and skeletonization, both the soma area and the total branch length of the microglia were successfully measured (88, 89).

Drug administration

Two microliters of minocycline (5 μ g/ μ l) and normal saline were immediately instilled into the lesion following SCI. Minocycline was administered in a solution of two to three drops, ensuring optimal drug immersion. Minocycline, a microglial inhibitor, was obtained from Sigma-Aldrich (m9511). TNF- α (Novus, NBP2-35185), IL-6 (MCE, HY-P7063), and IL-10 neutralizing antibody (MCE, HY-P990001) were applied at doses of 10 ng, 10 ng, and 2 μ g, respectively, dissolved in 2 μ l of minocycline solution. Two to three drops were added.

Primary astrocyte culture

Intact spinal cord tissues were extracted from 2-day-old C57BL/6 mice. The membrane tissue was carefully removed, and the minced spinal cord tissue was subsequently incubated in a 0.125% trypsin-EDTA solution (diluted in 1 \times phosphate-buffered saline (PBS)) obtained from Sigma-Aldrich (t4049) for 12 min at 37 $^{\circ}$ C. The cells were cultured in Gibco Dulbecco's modified Eagle's medium (Gibco, 11995065) supplemented with 10% fetal bovine serum (Gibco, A5670701) in a poly-D-lysine (PDL)-coated culture dish (Sigma-Aldrich,

Table 1
Primer sets are used for agarose gel electrophoresis

Gene	Forward (5'-3')
Pd1- Common	CACTATCCCACTGACCCCTTCA
Pd1- wild type	AGAAGGTGAGGGACCTCCAG
Pd1- mutant	CACAGGGTAGGCATGTAGCA

Microglial Pd1 disrupts glial scar formation after SCI

1 mg/ml, a003m) with an approximate surface area of 75 cm². Upon reaching confluence within 7 to 10 days, the cells were subjected to overnight agitation at 250 rpm on a shaker at 37 °C and subsequently reseeded onto PDL precoated 12-well or 24-well plates at 37 °C with a CO₂ concentration of 5% prior to conducting experiments.

Primary microglia culture

The aforementioned procedures were in accordance with those utilized for cultured astrocytes. Following cultivation at 37 °C for 16 to 18 days, the fused cell state was observed under an inverted microscope, revealing distinct round-shaped microglia exhibiting refractive properties that remained attached to the surface of the astrocytes. Subsequently, purified microglia were isolated by gently stirring them in serum-free medium for approximately 8 min followed by being reseeded into PDL-coated 12-well plates.

Small interfering RNA transfection and LPS injection

Microglia were transfected with Pd1 siRNA at concentrations of 5 nM and 50 nM, as well as with NC small interfering RNA (siRNA) from RiboBio. Transfection was performed using RNAiMAX (Invitrogen, 13778100) from Invitrogen for a period of 48 h. After that, the cells were exposed to LPS (Sigma–Aldrich, smb00610) at concentrations of 0 µg/ml, 1 µg/ml, and 5 µg/ml obtained from Sigma–Aldrich for 24 h. The Pd1 siRNA utilized in this study had the following specific sequence: 5'-CACAGAATATGCCACCAT-3'. For the NC siRNA, we used the sequence 5'-GGCTCTAGAAAAGCCTATGC-3'.

Scratch resistances

The astrocyte scratch model was previously employed (90). Briefly, a 10 µl pipette tip was used to create vertical scratches along the midline of the culture dish as astrocytes proliferated across the bottom surface of the porous plate. Subsequently, cellular debris was removed by washing with PBS following the scratching procedure. The conditioned medium was obtained by collecting the culture supernatant of microglia after siRNA transfection and LPS stimulation, which was subsequently utilized for astrocyte cultivation.

Quantitative real-time PCR

The injured spinal cord (T9–T10) tissues were collected at various time intervals following SCI, and RNA extraction was

performed using TRIzol reagent (Sigma–Aldrich, t9424). Later, reverse transcription of RNA was carried out using the HiScript III RT SuperMix for qPCR kit (Vazyme, R323–01). Primers, including a control for β-actin, were designed using the website <https://www.ncbi.nlm.nih.gov/> and synthesized by Genewiz. The primers utilized in this study for qPCR analysis can be found in Table 2 provided. ChamQ SYBR qPCR Master Mix (Vazyme, Q341–02) was chosen for qPCR amplification. The mRNA levels of specific genes were analyzed using the Step One Plus real-time PCR system, which generated amplification curves to evaluate primer efficiency for calculating relative gene expression levels.

Histological and immunohistochemical staining

The animals were perfused with physiological saline, followed by 4% paraformaldehyde *via* the left cardiac ventricle. The injured spinal cord (T9–T10) tissues were then postfixed for 8 h and immersed in a 30% sucrose solution at 4 °C until they sank. Cryostat-cut sections, measuring 12 µm in thickness, were gently placed on slides.

Hematoxylin and eosin staining

To enable a more comprehensive assessment of cellular and tissue structural modifications at the injury site, the spinal cords were subjected to H&E staining utilizing an H&E Staining Kit according to the instructions provided by the manufacturer (Abcam, ab245880).

Immunofluorescence staining

A blocking solution was prepared using 1% bovine serum albumin (Sigma–Aldrich, v900933) and 0.3% Triton X-100 (Sigma–Aldrich, t8787), which was applied for a period of 2 h to minimize any potential nonspecific binding. Next, the sections were incubated overnight at 4 °C with primary antibodies against Pd1 (Rabbit, Sigma–Aldrich Cat# PRS4065, RRID: AB_1855098 diluted to 1:500), Iba1 (Goat, NOVUS Cat# NB100–1028, RRID: AB_3148646, diluted to 1:100), GFAP (Mouse, MILLIPORE Cat# MAB360, RRID: AB_11212597, diluted to 1:1000), NeuN (Mouse, MILLIPORE Cat# MAB377, RRID: AB_2298772, diluted to 1:500), APC (Mouse, Sigma–Aldrich Cat# OP80, RRID: AB_2057371, diluted to 1:500), β-III tubulin (Mouse, Abcam Cat# ab52623, RRID: AB_869991, diluted to 1:1000), Iba1 (Rabbit, Wako Cat# 019–19741, RRID: AB_839504, diluted to 1:1000) and tmem119 (Mouse, Cell Signaling Technology Cat# 98778, RRID: AB_3676700, diluted

Table 2
Primer sets used for qPCR

Gene	Forward (5'-3')	Reverse (5'-3')
β-actin	CTCTCCAGCCTTCCTTCCT	CACCGATCCAGACGGAGTAT
CX3CR1	CTGTTATTTGGGCGACATTG	AACAGATTTCCCACCAGACC
IL-1β	TGTCTTGGCCGAGGACTAAG	TGGGCTGGACTGTTTCTAATG
IL-10	CTGGACAACATACTGCTAAC	AAATGCTCCTTGATTCTGG
IL-6	TCCATCCAGTTGCCTTCTTGG	CCACGATTTCCCAGAGAACATG
Pd1	GCCACCTTCACCTGCAGCTTG	AAACCGGCCTTCTGGTTGGGC
TNF-α	CCCCAAAGGGATGAGAAGTT	CACTTGGTGGTTTGCTACGA

to 1:100). Standard immunohistochemical techniques were employed for both single- and double-staining procedures. To visualize the primary antibodies effectively, the sections were subsequently exposed to their respective secondary antibodies (all from Jackson ImmunoResearch) at dilutions of 1:1000 each for a period of 2 h at room temperature. All antibodies' specificity were validated using a NC (where no primary antibody was added, while all other procedures remained identical) and confirmed by comparing the resulting sample morphology with that reported in the literature. A Nikon fluorescence microscope was used to capture images, which were further processed using ImageJ software.

Imaging analysis

The fluorescence microscopy setup was consistent for all images of sections stained with the same antibody, and ImageJ was utilized to project the image sections. Each group consisted of 4 to 7 mice, and eight tissue sections were prepared for each mouse, with each section being serially sectioned into five to six consecutive sections (12 μm in thickness). A single section was chosen from each animal, located at a comparable plane position, and two or three random areas within these chosen sections were examined. A square region (set size: 300 \times 300 pixel²) near the lesion core was chosen, and fluorescence intensity calculations were performed using the Analyze-Measure plugin in ImageJ following the threshold. The data were standardized to the mean value of their respective control groups. The experimenter responsible for the fluorescence statistics was blinded by the group allocation of each image.

Cytokine assay

The levels of specific cytokines secreted by microglia were quantified using a mouse cytokine microarray kit (R&D Systems, ARY006). A total of 500 μl of cell culture supernatant was collected from each group, including the NC siRNA group, NC siRNA + LPS (5 $\mu\text{g}/\text{ml}$) group, Pd1 siRNA (50 nM) group, and Pd1 siRNA (50 nM) + LPS (5 $\mu\text{g}/\text{ml}$) group. The particulate matter was eliminated through centrifugal separation. All steps were conducted in accordance with the guidelines provided by the manufacturer. To perform the assays, a Bio-Rad ChemiDoc system was utilized, and computer-assisted imaging was employed to measure relevant band intensities for densitometry analysis.

BMS scoring analysis

The BMS was used for the assessment of hind limb motor function following SCI in mice. Prior to assessment, a 30-min acclimation period was provided for the mice in the open field to familiarize themselves with the surroundings. Following the BMS scoring protocol, two trained evaluators independently and blinded assessed the motor function of each mouse's left and right hind limbs for a minimum of 3 minutes. They then calculated the mean score of the motion scores for the left and right hind limbs. The individuals responsible for conducting the behavioral test were blinded to the group affiliation of each mouse.

Experimental design and statistical analysis

All collected data from the mice were included in the analysis. For immunohistochemistry or behavioral analysis, we performed two or three separate repetitions. We conducted assessments for normality and homogeneity of variance prior to implementing parametric tests. When comparing the two groups, we employed unpaired Student's *t* test. Single-factor analysis of variance (ANOVA) was employed to compare multiple categories at a single time point, while two-way ANOVA was used to assess multiple categories across multiple time points. The subsequent analyses were performed using the Tukey, Dunnett, or Bonferroni correction methods. Statistical analysis was performed using GraphPad Prism 8.3.0 software. A significance level of $p < 0.05$ was used to determine significant differences among groups. The data were presented as the mean \pm standard deviation (SD).

Data availability

All data were provided in the figures, tables, and [supplementary information](#) in this paper.

Supporting information—This article contains supporting information.

Acknowledgments—We appreciate Springer Nature for language assistance.

Author contributions—Y. C., Z. L., X. S., M. L., L. X., T. Y., and G. C. methodology; Y. C., Z. L., X. S., M. L., T. Y., and G. C. investigation; Y. C. and G. C. writing—review and editing; Y. C. formal analysis; Y. C. writing—original draft; L. X. and G. C. conceptualization; L. X. and G. C. supervision; G. C. validation; G. C. project administration; G. C. funding acquisition.

Funding and additional information—This work was supported by funding to G. C. from the National Natural Science Foundation of China (32271054, 32070998), the National Key Research and Development Program of China (2022YFA1105900), Priority Academic Program Development of Jiangsu Higher Education Institutions (PAPD).

Conflict of interest—The authors declare that they have no conflicts of interest with the contents of this article.

Abbreviations—The abbreviations used are: APC, adenomatous polyposis coli clone 1; BMS, Basso Mouse Scale; CNS, central nervous system; dpi, days post injury; FBS, fetal bovine serum; IL, interleukin; LPS, lipopolysaccharide; NC, negative control; Pd1, programmed cell death protein 1; PDL, poly-D-lysine; qPCR, quantitative real-time PCR; ROS, reactive oxygen species; SCI, spinal cord injury; siRNA, small interfering RNA; TNF- α , tumor necrosis factor-alpha; TLR, Toll-like receptor.

References

- West, C. R., and Cragg, J. J. (2024) Getting to the heart of the problem in spinal cord injury. *J. Am. Coll. Cardiol.* **83**, 752–754
- Tran, A. P., Warren, P. M., and Silver, J. (2018) The biology of regeneration failure and success after spinal cord injury. *Physiol. Rev.* **98**, 881–917

Microglial Pd1 disrupts glial scar formation after SCI

- Tai, W., Wu, W., Wang, L. L., Ni, H., Chen, C., Yang, J., *et al.* (2021) *In vivo* reprogramming of NG2 glia enables adult neurogenesis and functional recovery following spinal cord injury. *Cell Stem Cell* **28**, 923–937.e924
- Silver, J., and Miller, J. H. (2004) Regeneration beyond the glial scar. *Nat. Rev. Neurosci.* **5**, 146–156
- Schäfer, M. K. E., and Tegeder, I. (2018) NG2/CSPG4 and progranulin in the posttraumatic glial scar. *Matrix Biol.* **68–69**, 571–588
- Anderson, M. A., Burda, J. E., Ren, Y., Ao, Y., O’Shea, T. M., Kawaguchi, R., *et al.* (2016) Astrocyte scar formation aids central nervous system axon regeneration. *Nature* **532**, 195–200
- Alliot, F., Godin, I., and Pessac, B. (1999) Microglia derive from progenitors, originating from the yolk sac, and which proliferate in the brain. *Brain Res. Dev. Brain Res.* **117**, 145–152
- Ginhoux, F., Greter, M., Leboeuf, M., Nandi, S., See, P., Gokhan, S., *et al.* (2010) Fate mapping analysis reveals that adult microglia derive from primitive macrophages. *Science* **330**, 841–845
- Greenhalgh, A. D., David, S., and Bennett, F. C. (2020) Immune cell regulation of glia during CNS injury and disease. *Nat. Rev. Neurosci.* **21**, 139–152
- Li, C., Wu, Z., Zhou, L., Shao, J., Hu, X., Xu, W., *et al.* (2022) Temporal and spatial cellular and molecular pathological alterations with single-cell resolution in the adult spinal cord after injury. *Signal. Transduct. Target Ther.* **7**, 65
- Fan, H., Tang, H. B., Shan, L. Q., Liu, S. C., Huang, D. G., Chen, X., *et al.* (2019) Quercetin prevents necroptosis of oligodendrocytes by inhibiting macrophages/microglia polarization to M1 phenotype after spinal cord injury in rats. *J. Neuroinflammation* **16**, 206
- Sun, F., Zhang, H., Huang, T., Shi, J., Wei, T., and Wang, Y. (2021) miRNA-221 regulates spinal cord injury-induced inflammatory response through targeting TNF- α expression. *Biomed. Res. Int.* **2021**, 6687963
- Cunha, M. I., Su, M., Cantuti-Castelvetri, L., Müller, S. A., Schifferer, M., Djannatian, M., *et al.* (2020) Pro-inflammatory activation following demyelination is required for myelin clearance and oligodendrogenesis. *J. Exp. Med.* **217**. <https://doi.org/10.1084/jem.20191390>
- Dougherty, K. D., Dreyfus, C. F., and Black, I. B. (2000) Brain-derived neurotrophic factor in astrocytes, oligodendrocytes, and microglia/macrophages after spinal cord injury. *Neurobiol. Dis.* **7**, 574–585
- Rotterman, T. M., Akhter, E. T., Lane, A. R., MacPherson, K. P., Garcia, V. V., Tansey, M. G., *et al.* (2019) Spinal motor circuit synaptic plasticity after peripheral nerve injury depends on microglia activation and a CCR2 mechanism. *J. Neurosci.* **39**, 3412–3433
- Jiang, D., Gong, F., Ge, X., Lv, C., Huang, C., Feng, S., *et al.* (2020) Neuron-derived exosomes-transmitted miR-124-3p protect traumatically injured spinal cord by suppressing the activation of neurotoxic microglia and astrocytes. *J. Nanobiotechnol.* **18**, 105
- Liddelow, S. A., Guttenplan, K. A., Clarke, L. E., Bennett, F. C., Bohlen, C. J., Schirmer, L., *et al.* (2017) Neurotoxic reactive astrocytes are induced by activated microglia. *Nature* **541**, 481–487
- Fan, H., Zhang, K., Shan, L., Kuang, F., Chen, K., Zhu, K., *et al.* (2016) Reactive astrocytes undergo M1 microglia/macrophages-induced necroptosis in spinal cord injury. *Mol. Neurodegener.* **11**, 14
- Jian, H., Wu, K., Lv, Y., Du, J., Hou, M., Zhang, C., *et al.* (2024) A critical role for microglia in regulating metabolic homeostasis and neural repair after spinal cord injury. *Free Radic. Biol. Med.* **225**, 469–481
- Brennan, F. H., Li, Y., Wang, C., Ma, A., Guo, Q., Li, Y., *et al.* (2022) Microglia coordinate cellular interactions during spinal cord repair in mice. *Nat. Commun.* **13**, 4096
- Zhou, Z. L., Xie, H., Tian, X. B., Xu, H. L., Li, W., Yao, S., *et al.* (2023) Microglial depletion impairs glial scar formation and aggravates inflammation partly by inhibiting STAT3 phosphorylation in astrocytes after spinal cord injury. *Neural Regen. Res.* **18**, 1325–1331
- Shinozaki, Y., Shibata, K., Yoshida, K., Shigetomi, E., Gachet, C., Ikenaka, K., *et al.* (2017) Transformation of astrocytes to a neuroprotective phenotype by microglia via P2Y(1) receptor downregulation. *Cell Rep.* **19**, 1151–1164
- Bellver-Landete, V., Bretheau, F., Mailhot, B., Vallières, N., Lessard, M., Janelle, M. E., *et al.* (2019) Microglia are an essential component of the neuroprotective scar that forms after spinal cord injury. *Nat. Commun.* **10**, 518
- Shinohara, T., Taniwaki, M., Ishida, Y., Kawaichi, M., and Honjo, T. (1994) Structure and chromosomal localization of the human PD-1 gene (PDCD1). *Genomics* **23**, 704–706
- Zhao, L., Ma, Y., Song, X., Wu, Y., Jin, P., and Chen, G. (2023) PD-1: a new candidate target for analgesic peptide design. *J. Pain* **24**, 1142–1150
- Le, D. T., Durham, J. N., Smith, K. N., Wang, H., Bartlett, B. R., Aulakh, L. K., *et al.* (2017) Mismatch repair deficiency predicts response of solid tumors to PD-1 blockade. *Science* **357**, 409–413
- Su, W., Saravia, J., Risch, I., Rankin, S., Guy, C., Chapman, N. M., *et al.* (2023) CXCR6 orchestrates brain CD8(+) T cell residency and limits mouse Alzheimer’s disease pathology. *Nat. Immunol.* **24**, 1735–1747
- Kim, J. E., Lee, R. P., Yazigi, E., Atta, L., Feghali, J., Pant, A., *et al.* (2024) Soluble PD-L1 reprograms blood monocytes to prevent cerebral edema and facilitate recovery after ischemic stroke. *Brain Behav. Immun.* **116**, 160–174
- Zhao, L., Luo, H., Ma, Y., Zhu, S., Wu, Y., Lu, M., *et al.* (2022) An analgesic peptide H-20 attenuates chronic pain via the PD-1 pathway with few adverse effects. *Proc. Natl. Acad. Sci. U. S. A.* **119**, e2204114119
- Linnerbauer, M., Beyer, T., Nirschl, L., Farrenkopf, D., Löbslein, L., Vandrey, O., *et al.* (2023) PD-L1 positive astrocytes attenuate inflammatory functions of PD-1 positive microglia in models of autoimmune neuroinflammation. *Nat. Commun.* **14**, 5555
- Xing, Z., Zuo, Z., Hu, D., Zheng, X., Wang, X., Yuan, L., *et al.* (2021) Influenza vaccine combined with moderate-dose PD1 blockade reduces amyloid- β accumulation and improves cognition in APP/PS1 mice. *Brain Behav. Immun.* **91**, 128–141
- Bodhankar, S., Chen, Y., Lapato, A., Dotson, A. L., Wang, J., Vandenbark, A. A., *et al.* (2015) PD-L1 monoclonal antibody treats ischemic stroke by controlling central nervous system inflammation. *Stroke* **46**, 2926–2934
- He, H., Zhou, Y., Zhou, Y., Zhuang, J., He, X., Wang, S., *et al.* (2018) Dexmedetomidine mitigates microglia-mediated neuroinflammation through upregulation of programmed cell death protein 1 in a rat spinal cord injury model. *J. Neurotrauma* **35**, 2591–2603
- Yao, A., Liu, F., Chen, K., Tang, L., Liu, L., Zhang, K., *et al.* (2014) Programmed death 1 deficiency induces the polarization of macrophages/microglia to the M1 phenotype after spinal cord injury in mice. *Neurotherapeutics* **11**, 636–650
- Liu, Y., Zhao, Y., Liao, X., Zhou, S., Guo, X., Yang, L., *et al.* (2024) PD-1 deficiency aggravates spinal cord injury by regulating the reprogramming of NG2 glia and activating the Ngr/RhoA/ROCK signaling pathway. *Cell Signal.* **114**, 110978
- He, X., Lin, S., Yang, L., Tan, P., Ma, P., Qiu, P., *et al.* (2021) Programmed death protein 1 is essential for maintaining the anti-inflammatory function of infiltrating regulatory T cells in a murine spinal cord injury model. *J. Neuroimmunol.* **354**, 577546
- Zhou, X., Wahane, S., Friedl, M. S., Kluge, M., Friedel, C. C., Avramopoulos, K., *et al.* (2020) Microglia and macrophages promote corraling, wound compaction and recovery after spinal cord injury via Plexin-B2. *Nat. Neurosci.* **23**, 337–350
- Fu, H., Zhao, Y., Hu, D., Wang, S., Yu, T., and Zhang, L. (2020) Depletion of microglia exacerbates injury and impairs function recovery after spinal cord injury in mice. *Cell Death Dis.* **11**, 528
- Li, C., Wu, Z., Zhou, L., Shao, J., Hu, X., Xu, W., *et al.* (2022) Correction to: temporal and spatial cellular and molecular pathological alterations with single-cell resolution in the adult spinal cord after injury. *Signal. Transduct. Target Ther.* **7**, 154
- Kobayashi, K., Imagama, S., Ohgomori, T., Hirano, K., Uchimura, K., Sakamoto, K., *et al.* (2013) Minocycline selectively inhibits M1 polarization of microglia. *Cell Death Dis.* **4**, e525
- Henry, C. J., Huang, Y., Wynne, A., Hanke, M., Himler, J., Bailey, M. T., *et al.* (2008) Minocycline attenuates lipopolysaccharide (LPS)-induced neuroinflammation, sickness behavior, and anhedonia. *J. Neuroinflammation* **5**, 15
- Gordon, S. R., Maute, R. L., Dulken, B. W., Hutter, G., George, B. M., McCracken, M. N., *et al.* (2017) PD-1 expression by tumour-associated

- macrophages inhibits phagocytosis and tumour immunity. *Nature* **545**, 495–499
43. Wang, Z., Jiang, C., He, Q., Matsuda, M., Han, Q., Wang, K., *et al.* (2020) Anti-PD-1 treatment impairs opioid antinociception in rodents and nonhuman primates. *Sci. Transl. Med.* **12**, eaaw6471
 44. Zhao, J., Roberts, A., Wang, Z., Savage, J., and Ji, R. R. (2021) Emerging role of PD-1 in the central nervous system and brain diseases. *Neurosci. Bull.* **37**, 1188–1202
 45. Yang, T., Xing, L., Yu, W., Cai, Y., Cui, S., and Chen, G. (2020) Astrocytic reprogramming combined with rehabilitation strategy improves recovery from spinal cord injury. *FASEB J.* **34**, 15504–15515
 46. Hu, X., Xu, W., Ren, Y., Wang, Z., He, X., Huang, R., *et al.* (2023) Spinal cord injury: molecular mechanisms and therapeutic interventions. *Signal. Transduct. Target Ther.* **8**, 245
 47. Liu, X. Z., Xu, X. M., Hu, R., Du, C., Zhang, S. X., McDonald, J. W., *et al.* (1997) Neuronal and glial apoptosis after traumatic spinal cord injury. *J. Neurosci.* **17**, 5395–5406
 48. Zusso, M., Lunardi, V., Franceschini, D., Pagetta, A., Lo, R., Stifani, S., *et al.* (2019) Ciprofloxacin and levofloxacin attenuate microglia inflammatory response via TLR4/NF- κ B pathway. *J. Neuroinflammation* **16**, 148
 49. Chen, W. F., Shih, Y. H., Liu, H. C., Cheng, C. I., Chang, C. I., Chen, C. Y., *et al.* (2022) 6-methoxyflavone suppresses neuroinflammation in lipopolysaccharide-stimulated microglia through the inhibition of TLR4/MyD88/p38 MAPK/NF- κ B dependent pathways and the activation of HO-1/NQO-1 signaling. *Phytomedicine* **99**, 154025
 50. Yang, L., Zhou, R., Tong, Y., Chen, P., Shen, Y., Miao, S., *et al.* (2020) Neuroprotection by dihydrotestosterone in LPS-induced neuroinflammation. *Neurobiol. Dis.* **140**, 104814
 51. Allen, A. R. (1911) Surgery of experimental lesion of spinal cord equivalent to crush injury of fracture dislocation of spinal column: a preliminary report. *JAMA*, 878–880
 52. Wanner, I. B., Anderson, M. A., Song, B., Levine, J., Fernandez, A., Gray-Thompson, Z., *et al.* (2013) Glial scar borders are formed by newly proliferated, elongated astrocytes that interact to corral inflammatory and fibrotic cells via STAT3-dependent mechanisms after spinal cord injury. *J. Neurosci.* **33**, 12870–12886
 53. Kent, S. A., and Miron, V. E. (2024) Microglia regulation of central nervous system myelin health and regeneration. *Nat. Rev. Immunol.* **24**, 49–63
 54. Willis, E. F., MacDonald, K. P. A., Nguyen, Q. H., Garrido, A. L., Gillespie, E. R., Harley, S. B. R., *et al.* (2020) Repopulating microglia promote brain repair in an IL-6-dependent manner. *Cell* **180**, 833–846.e816
 55. Prinz, M., Jung, S., and Priller, J. (2019) Microglia biology: one century of evolving concepts. *Cell* **179**, 292–311
 56. Colonna, M., and Butovsky, O. (2017) Microglia function in the central nervous system during health and neurodegeneration. *Annu. Rev. Immunol.* **35**, 441–468
 57. Shultz, R. B., and Zhong, Y. (2017) Minocycline targets multiple secondary injury mechanisms in traumatic spinal cord injury. *Neural Regen. Res.* **12**, 702–713
 58. Bassett, B., Subramaniam, S., Fan, Y., Varney, S., Pan, H., Carneiro, A. M. D., *et al.* (2021) Minocycline alleviates depression-like symptoms by rescuing decrease in neurogenesis in dorsal hippocampus via blocking microglia activation/phagocytosis. *Brain Behav. Immun.* **91**, 519–530
 59. Lee, S. M., Yune, T. Y., Kim, S. J., Park, D. W., Lee, Y. K., Kim, Y. C., *et al.* (2003) Minocycline reduces cell death and improves functional recovery after traumatic spinal cord injury in the rat. *J. Neurotrauma* **20**, 1017–1027
 60. Pi, R., Li, W., Lee, N. T., Chan, H. H., Pu, Y., Chan, L. N., *et al.* (2004) Minocycline prevents glutamate-induced apoptosis of cerebellar granule neurons by differential regulation of p38 and Akt pathways. *J. Neurochem.* **91**, 1219–1230
 61. Takeda, M., Kawaguchi, M., Kumatoriya, T., Horiuchi, T., Watanabe, K., Inoue, S., *et al.* (2011) Effects of minocycline on hind-limb motor function and gray and white matter injury after spinal cord ischemia in rats. *Spine (Phila Pa 1976)* **36**, 1919–1924
 62. Stirling, D. P., Khodarahmi, K., Liu, J., McPhail, L. T., McBride, C. B., Steeves, J. D., *et al.* (2004) Minocycline treatment reduces delayed oligodendrocyte death, attenuates axonal dieback, and improves functional outcome after spinal cord injury. *J. Neurosci.* **24**, 2182–2190
 63. Li, Y., He, X., Kawaguchi, R., Zhang, Y., Wang, Q., Monavarfeshani, A., *et al.* (2020) Microglia-organized scar-free spinal cord repair in neonatal mice. *Nature* **587**, 613–618
 64. Adams, K. L., and Gallo, V. (2018) The diversity and disparity of the glial scar. *Nat. Neurosci.* **21**, 9–15
 65. Bradbury, E. J., and Burnside, E. R. (2019) Moving beyond the glial scar for spinal cord repair. *Nat. Commun.* **10**, 3879
 66. Vanganswinkel, T., Lemmens, S., Tiane, A., Geurts, N., Dooley, D., Vanmierlo, T., *et al.* (2023) Therapeutic administration of mouse mast cell protease 6 improves functional recovery after traumatic spinal cord injury in mice by promoting remyelination and reducing glial scar formation. *FASEB J.* **37**, e22939
 67. Liu, F. T., Xu, S. M., Xiang, Z. H., Li, X. N., Li, J., Yuan, H. B., *et al.* (2014) Molecular hydrogen suppresses reactive astrogliosis related to oxidative injury during spinal cord injury in rats. *CNS Neurosci. Ther.* **20**, 778–786
 68. Goldshmit, Y., Jona, G., Schmukler, E., Solomon, S., Pinkas-Kramarski, R., and Ruban, A. (2018) Blood glutamate scavenger as a novel neuroprotective treatment in spinal cord injury. *J Neurotrauma* **35**, 2581–2590
 69. Wilhelmsson, U., Li, L., Pekna, M., Berthold, C. H., Blom, S., Eliasson, C., *et al.* (2004) Absence of glial fibrillary acidic protein and vimentin prevents hypertrophy of astrocytic processes and improves post-traumatic regeneration. *J. Neurosci.* **24**, 5016–5021
 70. Okada, S., Nakamura, M., Katoh, H., Miyao, T., Shimazaki, T., Ishii, K., *et al.* (2006) Conditional ablation of Stat3 or Socs3 discloses a dual role for reactive astrocytes after spinal cord injury. *Nat. Med.* **12**, 829–834
 71. Bu, X., Juneja, V. R., Reynolds, C. G., Mahoney, K. M., Bu, M. T., McGuire, K. A., *et al.* (2021) Monitoring PD-1 phosphorylation to evaluate PD-1 signaling during antitumor immune responses. *Cancer Immunol. Res.* **9**, 1465–1475
 72. Han, R., Luo, J., Shi, Y., Yao, Y., and Hao, J. (2017) PD-L1 (Programmed death ligand 1) protects against experimental intracerebral hemorrhage-induced brain injury. *Stroke* **48**, 2255–2262
 73. Rosenzweig, N., Dvir-Szternfeld, R., Tsitsou-Kampeli, A., Keren-Shaul, H., Ben-Yehuda, H., Weill-Raynal, P., *et al.* (2019) PD-1/PD-L1 checkpoint blockade harnesses monocyte-derived macrophages to combat cognitive impairment in a tauopathy mouse model. *Nat. Commun.* **10**, 465
 74. Zhao, J., Bang, S., Furutani, K., McGinnis, A., Jiang, C., Roberts, A., *et al.* (2023) PD-L1/PD-1 checkpoint pathway regulates hippocampal neuronal excitability and learning and memory behavior. *Neuron* **111**, 2709–2726. e2709
 75. Chen, G., Kim, Y. H., Li, H., Luo, H., Liu, D. L., Zhang, Z. J., *et al.* (2017) PD-L1 inhibits acute and chronic pain by suppressing nociceptive neuron activity via PD-1. *Nat. Neurosci.* **20**, 917–926
 76. Wang, K., Gu, Y., Liao, Y., Bang, S., Donnelly, C. R., Chen, O., *et al.* (2020) PD-1 blockade inhibits osteoclast formation and murine bone cancer pain. *J. Clin. Invest.* **130**, 3603–3620
 77. Kleffel, S., Posch, C., Barthel, S. R., Mueller, H., Schlapbach, C., Guenova, E., *et al.* (2015) Melanoma cell-intrinsic PD-1 receptor functions promote tumor growth. *Cell* **162**, 1242–1256
 78. Shen, H., Gu, J., Liu, X., and Song, M. (2024) Small nucleolar RNA host gene 1 silencing inhibits the lipopolysaccharide-induced microglial apoptosis and inflammation. *Cell Mol. Biol.* **70**, 182–186
 79. Xiao, S., Zhang, Y., Liu, Z., Li, A., Tong, W., Xiong, X., *et al.* (2023) Alpinetin inhibits neuroinflammation and neuronal apoptosis via targeting the JAK2/STAT3 signaling pathway in spinal cord injury. *CNS Neurosci. Ther.* **29**, 1094–1108
 80. Liu, W., Rong, Y., Wang, J., Zhou, Z., Ge, X., Ji, C., *et al.* (2020) Exosome-shuttled miR-216a-5p from hypoxic preconditioned mesenchymal stem cells repair traumatic spinal cord injury by shifting microglial M1/M2 polarization. *J. Neuroinflammation* **17**, 47
 81. Rong, Y., Wang, J., Hu, T., Shi, Z., Lang, C., Liu, W., *et al.* (2024) Ginsenoside Rg1 regulates immune microenvironment and neurological recovery after spinal cord injury through MYCBP2 delivery via neuronal cell-derived extracellular vesicles. *Adv. Sci. (Weinh)* **11**, e2402114

Microglial Pd1 disrupts glial scar formation after SCI

82. Wu, F., Zhang, P., and Zhou, G. (2023) The involvement of EGR1 in neuron apoptosis in the *in vitro* model of spinal cord injury via BTG2 up-regulation. *Neurol. Res.* **45**, 646–654
83. Boomkamp, S. D., Riehle, M. O., Wood, J., Olson, M. F., and Barnett, S. C. (2012) The development of a rat *in vitro* model of spinal cord injury demonstrating the additive effects of Rho and ROCK inhibitors on neurite outgrowth and myelination. *Glia* **60**, 441–456
84. Sabogal-Guáqueta, A. M., Marmolejo-Garza, A., Trombetta-Lima, M., Oun, A., Hunneman, J., Chen, T., *et al.* (2023) Species-specific metabolic reprogramming in human and mouse microglia during inflammatory pathway induction. *Nat. Commun.* **14**, 6454
85. Marschallinger, J., Iram, T., Zardeneta, M., Lee, S. E., Lehallier, B., Haney, M. S., *et al.* (2020) Lipid-droplet-accumulating microglia represent a dysfunctional and proinflammatory state in the aging brain. *Nat. Neurosci.* **23**, 194–208
86. Kim, J., Sullivan, O., Lee, K., Jao, J., Tamayo, J., Madany, A. M., *et al.* (2024) Repeated LPS induces training and tolerance of microglial responses across brain regions. *J. Neuroinflammation* **21**, 233
87. Faber-Elman, A., Lavie, V., Schwartz, I., Shaltiel, S., and Schwartz, M. (1995) Vitronectin overrides a negative effect of TNF-alpha on astrocyte migration. *FASEB J.* **9**, 1605–1613
88. Young, K., and Morrison, H. (2018) Quantifying microglia morphology from photomicrographs of immunohistochemistry prepared tissue using ImageJ. *J. Vis. Exp.* <https://doi.org/10.3791/57648>
89. Dong, H., Zhang, X., Duan, Y., He, Y., Zhao, J., Wang, Z., *et al.* (2024) Hypoxia inducible factor-1 α regulates microglial innate immune memory and the pathology of Parkinson's disease. *J. Neuroinflammation* **21**, 80
90. Ropper, A. E., Zeng, X., Anderson, J. E., Yu, D., Han, L., Haragopal, H., *et al.* (2015) An efficient device to experimentally model compression injury of mammalian spinal cord. *Exp. Neurol.* **271**, 515–523